

One Cognitive Loop Is Enough: SODA unlocks Pure-Text Spatial Reasoning in Large Language Models

Anonymous ACL submission

Abstract

Currently, large language models (LLMs) have significant limitations in spatial reasoning, particularly in the absence of visual input. To address this issue, we introduce **SODA** (Spatial OODA), which draws inspiration from the OODA cognitive loop (Observe, Orient, Decide, Act), originally designed to enhance human decision-making in dynamic environments. Specifically, we embed the OODA loop into multiple control tasks, generating the *SPOD-143k* dataset, and successfully integrate it into LLMs through a two-phase and spatio-aware training strategy (SFT and GRPO). Furthermore, to fill the gap in evaluating spatial reasoning in purely text-based LLMs, we introduce the *SPOD-Bench* benchmark, including multiple tasks divided into three levels of difficulty. Experimental results show that **SODA** significantly enhances the spatial reasoning capabilities of LLMs across testing scenarios including *SPOD-Bench*, *SPACE* and applications, providing a replicable and effective paradigm for improving the spatial cognition of LLMs.

1 Introduction

Despite their strong general language capabilities (Brown et al., 2020; Achiam et al., 2023), Large Language Models (LLMs) are hindered by hallucinations and insensitivity to logical symbols (Ramakrishnan et al., 2025; Huang et al., 2025; Bai et al., 2025), leading to errors in basic numerical comparisons like distinguishing 9.11 from 9.9 (Xie, 2025; Liu and Fang, 2025). LLMs also show significant limitations in spatial cognitive tasks requiring spatial relations, directionality, and geometric reasoning (Bubeck et al., 2023; Li et al., 2024; Hendrycks et al., 2021), such as natural language navigation (Tikhonov, 2024). Their performance varies across spatial structures, and they struggle with complex spatial reasoning (Wu et al., 2024). Current research often relies on costly vision-language or robotic sensory data, which

leads to high development expenses, poor transferability, and a disregard for logical consistency in reasoning (Yamada et al., 2024; Chen et al., 2024; Stogiannidis et al., 2025; Yin et al., 2025; Brohan et al., 2023; Li et al., 2022; Shu et al., 2025; Khemlani et al., 2025). Consequently, existing LLMs face significant challenges in performing text-driven spatial reasoning without external sensory input (Driess et al., 2023; Ahn et al., 2022; Surís et al., 2023).

To address this, we draw inspiration from the OODA (Observe, Orient, Decide, Act) loop, a cognitive model that provides a structured framework for simulating biological spatial cognitive processes (Enck, 2012). Spatial cognition is fundamentally a Perception-Action Cycle (Fuster, 2004; Egelhaaf and Lindemann, 2025; Takahashi et al., 2024; Ji et al., 2025; Bollig et al., 2024; Dong and Fiete, 2024; Collett et al., 2025). By integrating the OODA loop, LLMs can simulate this process using only language: "Observe" to parse the environment, "Orient" to localize, "Decide" to plan paths, and "Act" to simulate task completion. Building on this, we introduce SODA (Spatial OODA) to systematically enhance LLM spatial reasoning. First, we created *SPOD-143k*, a large-scale pure-text spatial dataset of 143,000 question-answer pairs across 17 categories, integrating the OODA framework into the intermediate reasoning process of the data. We then embed this framework into LLMs via Supervised Fine-Tuning (SFT) and Group Relative Policy Optimization (GRPO(Shao et al., 2024)) on *SPOD-143k*, enabling structured spatial reasoning purely through language.

Furthermore, to address the lack of benchmarks for spatial reasoning without visual input, we introduce *SPOD-Bench*, a text-only benchmark with 13 categories across 3 difficulty levels. We applied SODA to Qwen3-4B and Qwen3-14B, conducting comparative experiments on *SPOD-Bench*, the *SPACE* dataset (Ramakrishnan et al., 2025), and

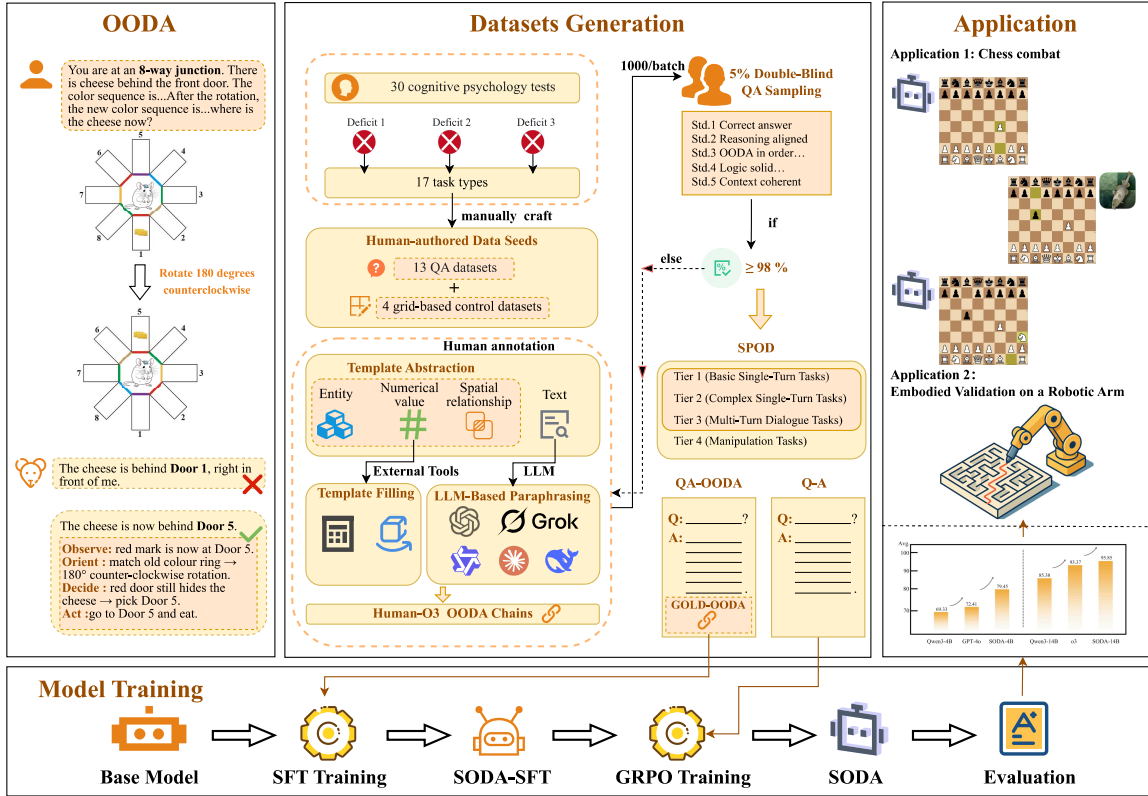


Figure 1: SODA workflow: OODA reasoning, SPOD dataset generation, training and evaluation pipeline, and applications. Left: An example OODA loop (Observe → Orient → Decide → Act) that lets the model correct a spatial mistake after a 180-degree rotation. Middle: How the SPOD dataset is built—from small human-written seeds, through template expansion and LLM paraphrasing, with 5 % double-blind quality checks—covering 17 spatial task types. Right: Two applications that use the trained model: playing chess against Stockfish and guiding a real robotic arm through a maze. Bottom: Training pipeline—Base model → SFT → SODA-SFT → GRPO fine-tuning → final SODA model → evaluation.

a Chess Combat test. As illustrated in Figure 1, SODA-enhanced models perform on par with or even surpass existing LLMs. This demonstrates an effective and replicable paradigm for enhancing the spatial cognition of smaller LLMs.

To conclude, our contributions are as follows: (i) We introduce the OODA cognitive loop, offering a new paradigm for pure-text spatial reasoning in LLMs. (ii) We constructed a large-scale, pure-text dataset, *SPOD-143k*, and deeply integrated the OODA framework into model reasoning via a two-stage training pipeline. (iii) We developed the first diverse and hierarchical pure-text spatial reasoning benchmark, *SPOD-Bench*. (iv) Extensive experiments on *SPOD-Bench*, public datasets, and real-world applications demonstrate the performance of the proposed method.

2 Related Work

2.1 Spatial Cognition and Reasoning in LLMs

Spatial cognition is a vital component of human intelligence, encompassing spatial perception, rea-

soning, control, and language understanding. In the context of LLMs, spatial perception involves sensing the spatial position of objects (Xuan et al., 2024; Xu et al., 2024), spatial reasoning pertains to the logical deduction of spatial relationships (Rodionov et al., 2025; Wang et al., 2024), spatial control is manifested in object path planning and navigation (Aghzal et al., 2025; Koh et al., 2021), and spatial language understanding is the core ability for LLMs to comprehend spatial concepts (Du et al., 2024). Human children gradually develop spatial cognitive abilities through activities such as playing with building blocks and cultivating a sense of direction (Lee et al., 2012; Yang and Pan, 2021). These abilities help humans perceive and understand the world. Similarly, for large language models, they are also crucial for understanding spatial environments. To this end, we have constructed a dataset covering spatial perception, reasoning, path planning and navigation, and spatial language understanding to train the spatial cognitive abilities of LLMs.

Spatial reasoning refers to the construction and

manipulation of spatial relationships between objects based on linguistic expressions or symbolic inputs to complete inferential and decision-making tasks such as path planning, scene comprehension, and layout judgments. While some studies indicate that current cutting-edge models face challenges in large-scale spatial cognition, with performance below human levels (Ramakrishnan et al., 2025), LLMs are capable of building limited spatial cognition from unstructured language to support reasoning. Thus, we introduce the OODA loop to enable models to excel in spatial perception, reasoning, path planning, and spatial language understanding.

2.2 OODA

OODA was originally proposed to enhance human decision-making capabilities in adversarial and dynamic environments (Boyd, 1996; Brehmer, 2005). It consists of four parts: Observe, Orient, Decide, and Act. Observe and Orient correspond to the Perception stage in the Perception-Action Cycle, while Decide and Act correspond to the Action stage (Endsley, 2017). The Observe phase collects internal and external environmental data to build a knowledge graph of the current situation (Bala et al., 2024). The Orient phase analyzes, interprets, and localizes the observed information, with its core lying in the cognitive understanding and interpretation of the task (Abdollahian and Jeffries, 2024). The Decide phase involves choosing among different courses of action based on the understanding of the environment and context, determining the next plan of action. Finally, the Act phase implements the decision and feeds its results back into the next cycle (Bhatt and Ganatra, 2022). In spatial cognition and movement processes, OODA can rapidly iterate information (Bala et al., 2024), greatly improving action accuracy, especially when used in agent collaboration to achieve intelligent spatial decision-making without any extra external prompts (Nguyen et al., 2024; Chang et al., 2024).

3 Approach

We propose **SODA (Spatial OODA)**, which enhances the spatial cognition and reasoning abilities of LLMs by constructing a large-scale text-based spatial dataset, *SPOD-143k*, and embedding the OODA framework. To address the lack of spatial reasoning benchmarks for models without visual input, we designed *SPOD-Bench*. Next, we will first introduce the premise of **SODA**, how OODA-

guided prompt chains are used for reasoning, and then describe the composition and construction process of the two datasets.

3.1 Preliminary (OODA-guided Prompt Chain)

We propose a reasoning framework based on the OODA loop that does not involve training or changes to the model’s internal structure. A question extractor generates an initial blueprint for the four stages (Observe, Orient, Decide, Act), and a self-instructing prompt generator creates customized prompts for each stage. During the reasoning process, large language models execute the four stages sequentially, enhancing the accuracy and consistency of spatial text tasks without the need for manual prompt tuning, while ensuring traceability.

As shown in Table 1, the experimental results indicate that, without additional training or reinforcement learning, this framework significantly improves the accuracy of GPT-5 and Qwen3-4B across five test sets, with first-answer accuracy rising from 0.252 to 0.813, validating the effectiveness of OODA. However, due to the inference latency caused by multiple agent calls, response efficiency still needs improvement. Therefore, we propose SODA, embedding OODA internally into the model. Below, we first introduce how to construct appropriate training and testing datasets using OODA, and then describe the two-stage training pipeline.

Model	DR	MPR	DPR	MRM	CMM
<i>GPT-5</i>					
Without OC	77.5	64.5	65.2	30.3	49.8
With OC	94.7	80.6	83.3	50.9	87.0
Gain	+17.2	+16.1	+18.1	+20.6	+37.2
<i>Qwen3-4B</i>					
Without OC	42.0	38.3	70.6	34.3	34.5
With OC	78.1	56.9	88.2	52.8	51.5
Gain	+36.1	+18.6	+17.6	+18.5	+17.0
<i>o3</i>					
Without OC	52.0	95.0	92.0	99.9	92.6

Table 1: Performance gains with trainfree O-O-D-A 4-steps Reasoning Chain (OC) enhancement across parts of spatial reasoning tasks with o3 model performance provided for reference. Tasks abbreviations refer to the Dataset Overview below.

3.2 SPOD

To assess the spatial reasoning capabilities of LLMs without visual input, we designed the *SPOD-Bench* based on comparative and developmental psychology. *SPOD-Bench* explores the core representations of language models in a text-based mode, ensuring traceability of the reasoning process. At the same time, to deeply integrate OODA abilities into the LLM, we propose *SPOD-143k*, which contains 64k more data entries than *SPOD-Bench* and integrates datasets for four additional control tasks (which we also constructed ourselves, with the process outlined later). Each data entry of *SPOD-143k* is designed to include a gold-standard OODA chain, thereby providing complete cognitive tracking and guiding the model’s internal OODA reasoning capabilities.

3.2.1 Dataset Overview

The *SPOD-Bench* includes 13 task types, covering basic spatial perception to complex multi-step control tasks. Specifically, based on the three common defects identified in LLM spatial reasoning (detailed in the appendix), the dataset is divided into three layers according to the difficulty of the defects:

Tier 1 (Basic Single-Turn Tasks). Inspired by geometric foundational defects, these tasks involve the model misjudging basic concepts, such as Euclidean distances and left-right relationships. To rebuild this foundational knowledge, we provide four single-step datasets: *Memory Path (MP)*, *Object Location Distance (OLD)*, *Relative Direction (RD)*, *Shortest Path (SP)*.

Tier 2 (Complex Single-Turn Tasks). Inspired by unstable spatial transformation defects, such as rotation, reflection, and coordinate translation, which often disrupt the model’s internal reference framework, we provide five datasets that require explicit mental transformations: *Packing Shapes (PS)*, *Mental Rotation (MR)*, *Double-Point Relation (DPR)*, *Multi-Point Relation (MPR)*, *Door Rotation (DR)*.

Tier 3 (Multi-Turn Dialogue Tasks). Inspired by long-term planning defects, these tasks reflect the premature interruption of multi-step decision chains. Four datasets require continuous state tracking and planning depth: *Door Rotation Multi-turn (DRM)*, *Spatial Relation Multi-turn (SRM)*, *Coordinates Movement Multi-turn (CMM)*, *Mental Rotation Multi-turn (MRM)*.

Additional control tasks of SPOD-143k.

Based on the *SPOD-Bench*, *SPOD-143k* includes four interactive control **grid world maze tasks**. They are parameterized by grid sizes (3, 5, 7, 9) and obstacle density, covering four different setups: OP, FOP, MCF, and MCO. Examples of tasks for Tier 1-3, and grid-world maze are shown in Figure 2, along with the data size for each *SPOD-143k*.

3.2.2 SPOD-Bench Construction

We use external tools and algorithmic programs to generate values, entities, and spatial relationships in QA tasks. A lightweight pipeline in Python handles this: Shapely (Gillies et al., 2024) creates and transforms geometric objects for ground-truth relations, GeoPandas (GeoPandas 0.15.0) manages CRS conversion and nearest-neighbour queries, and NetworkX (Hagberg et al., 2025) provides shortest paths on graphs. Scalar results are checked with NumPy and manually verified before writing each QA pair and its gold OODA chain to JSON for training and evaluation.

3.2.3 SPOD-143k Construction

To ensure scalability and quality, we constructed a high-quality dataset containing OODA reasoning through three steps: data seed annotation, extended generation of instances, and quality control. This process resulted in approximately 143k instances.

- **Step 1: Data Seed Annotation.** For the 13 basic tasks, we generated 100 entries per task as golden data seeds, similar to the test set construction. For control tasks, we use the A* algorithm to generate four interactive grid-world maze datasets (details in the appendix).
- **Step 2: Human-Machine Data Expansion.** We expanded the dataset using high-quality seed data through a human-machine pipeline. Each seed instance was abstracted into a general template, separating logical structure from lexical form. These templates were scaled using scripts and external tools, with LLMs rewriting the instances for lexical diversity. Finally, the golden standard OODA chains were generated by providing questions and real answers with powerful LLMs.
- **Step 3: Iterative Quality Control.** We generated 1,000 entries at a time and randomly selected 5% (50 items) for double-blind manual inspection. A batch was retained only if at least 98% of the inspected items met the

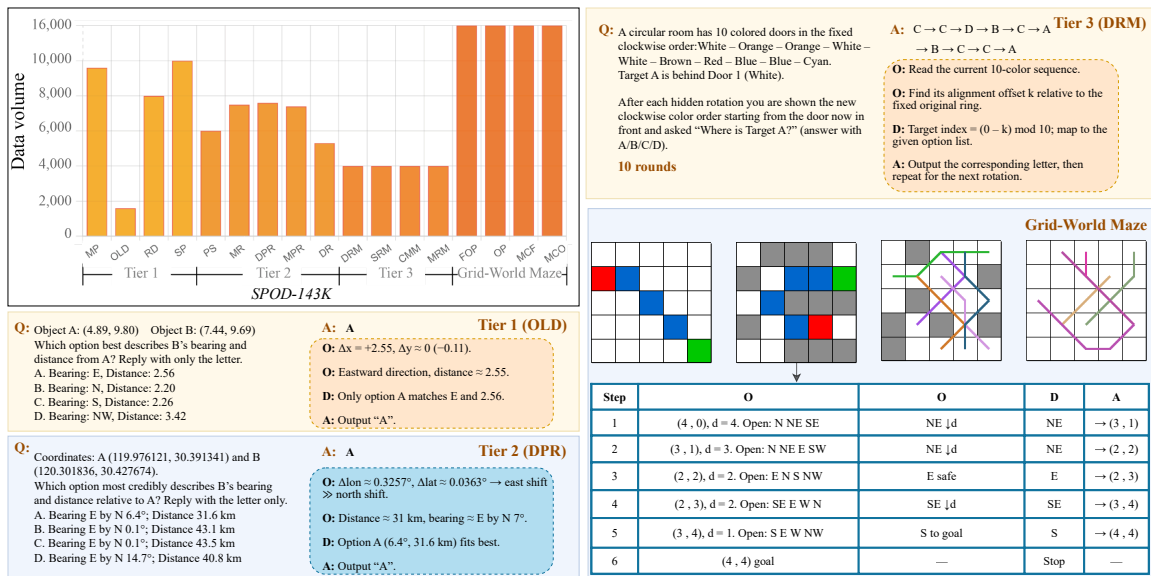


Figure 2: Data Volume and Examples of *SPOD-143k*.

following five standards: (i) correct answer; (ii) reasoning matches the answer; (iii) correct OODA stage order; (iv) logically rigorous reasoning chain; (v) consistent spatial context tracking in multi-turn tasks.

3.3 SODA

3.3.1 Supervised Fine-Tuning (SFT)

We begin with a pre-trained language model and fine-tune it on *SPOD-143k*. This step provides the model with core spatial concepts (such as orientation, rotation, pathfinding, and stacking) and integrates the OODA process into the model's reasoning while retaining the strengths of the base model.

3.3.2 Group Relative Policy Optimization (GRPO)

Based on the SFT checkpoint, we applied GRPO for reinforcement learning, also on *SPOD-143k*. For each question, the model proposes multiple candidate answers, evaluates their correctness and OODA chain quality, ranks them, and updates its parameters based on this ranking. The group-ranking signal provides a lightweight, effective optimization without needing a critic. The reward function uses a dual-reward system, focusing on both "Conclusion Accuracy" and "Format Accuracy."

$$r_i = r_{\text{ans}}(o_i) + r_{\text{ooda}}(o_i).$$

- The Conclusion Accuracy Reward r_{ans} . We use a regularization matching method, assigning a reward of +1.0 for completely correct answers, -1.0 for incorrect answers, and -1.4 for answers with no reasoning.

- The Format Accuracy Reward r_{ooda} . We check whether the generated text sequentially includes the four reasoning stages: Observe, Orient, Decide, and Act. Each correctly included stage is rewarded with +0.1, while missing stages, reversed order, or logical jumps are penalized with -0.1, so $r_{\text{ooda}} \in [-0.4, 0.4]$.

Thus, the original reward range for a single candidate is $[-1.8, 1.4]$. This design aims to suppress the model's tendency to miss the OODA thinking chain, extend the model's thinking length within the OODA process, and further improve accuracy on top of the original training foundation.

4 Experiments

This section assesses the performance of **SODA** on *SPOD-Bench* and *SPACE*, highlighting its advantages. It further demonstrates the generalizability by evaluating its performance in practical applications, including Chess Combat and robotic arm tasks. Additionally, the effectiveness of SODA is validated through sensitivity and ablation analysis.

4.1 Experiment Setup

We trained the Qwen3-4B and Qwen3-14B models during the SFT process, which ran for 3 epochs using the AdamW optimizer. In the GRPO process, 2 epochs were set with a learning rate of $2e-5$, 0.03 warm-up steps, and cosine learning rate decay. The training data for both stages are derived from *SPOD-143k*. The training data for control abilities included tasks involving the movement of multiple objects.

Model	Basic Single-Turn				Complex Single-Turn					Multi-Turn			
	OLD	SP	RD	MP	PS	MR	MPR	DPR	DR	DRM	SRM	MRM	CMM
<i>Non-Reasoning Models</i>													
GPT-5 nano	97.6	93.5	92.8	96.2	65.1	56.2	46.5	58.9	68.1	29.1	47.0	25.0	34.1
DeepSeek-v3	97.5	93.9	92.9	<u>98.6</u>	66.7	61.8	46.9	57.9	70.3	27.1	48.3	26.3	36.9
Qwen2.5-14B-Instr.	98.4	83.7	91.2	93.6	98.1	74.9	60.4	65.8	45.3	40.2	49.4	<u>28.6</u>	42.8
GPT-5	<u>98.9</u>	95.2	<u>96.5</u>	97.9	81.5	88.6	63.0	64.1	76.2	47.1	62.3	28.3	47.5
Claude-3-7-sonnet	98.4	98.1	84.9	95.8	100.0	<u>92.9</u>	<u>86.7</u>	<u>75.3</u>	<u>77.3</u>	<u>76.2</u>	<u>87.1</u>	27.8	<u>48.2</u>
<i>Reasoning Models</i>													
o4-mini	100.0	97.3	97.1	95.8	100.0	94.7	<u>97.4</u>	88.4	26.9	96.9	93.2	99.7	94.1
Grok 4.1	99.3	96.8	98.1	<u>98.7</u>	95.0	95.1	70.0	80.2	83.1	55.0	61.2	33.1	44.8
Claude Opus 4.5	99.7	97.5	98.2	98.5	98.8	95.5	96.0	93.0	<u>94.9</u>	98.0	95.5	97.5	94.5
o3	100.0	<u>97.8</u>	98.4	93.9	100.0	94.1	95.3	92.5	52.9	<u>99.6</u>	<u>96.8</u>	99.9	92.6
DeepSeek-R1	100.0	90.7	99.3	94.2	99.6	92.8	94.8	85.2	33.4	83.1	92.7	98.9	95.9
Qwen3-4B	93.8	66.3	95.7	89.8	98.4	91.9	73.6	87.9	42.1	38.3	54.7	34.3	34.5
Qwen3-14B	100.0	96.6	100.0	94.2	100.0	<u>95.7</u>	91.6	<u>93.3</u>	63.9	80.1	79.7	42.8	72.1
<i>Our Models based on Qwen3</i>													
SODA-4B	99.5	82.1	97.3	88.9	100.0	93.6	98.3	98.6	46.7	60.3	59.4	31.4	76.8
SODA-14B	100.0	<u>97.6</u>	<u>99.8</u>	99.3	100.0	98.2	100.0	100.0	95.1	99.8	97.3	<u>63.9</u>	<u>95.1</u>

Table 2: Overall accuracy (%) of baseline LLMs, reasoning-enhanced LLMs, and our SODA models on the 13-task SPOD-Bench. Tasks are grouped by tier: Basic Single-Turn (**OLD**, **SP**, **RD**, **MP**), Complex Single-Turn (**PS**, **MR**, **MPR**, **DPR**, **DR**), and Multi-Turn (**DRM**, **SRM**, **MRM**, **CMM**). The **best** score in each column is shown in **bold**; the best score in each sub-column is underlined. Higher values indicate better spatial-cognition performance.

4.2 Evaluating in SPOD-Bench

To establish a performance baseline, we evaluated several mainstream large-scale language models, including mainstream Reasoning and non-Reasoning in OpenAI (OpenAI, 2023, 2025), Claude (Anthropic, 2025,?), DeepSeek (Guo et al., 2025; DeepSeek-AI et al., 2025), Qwen (Yang et al., 2025) and Grok (xAI, 2025). The results are shown in Table 2.

Overall Performance Overview Both the 4B and 14B models demonstrate a comprehensive performance improvement with **SODA**, particularly in movement and path planning tasks. The SODA-4B model achieved an accuracy of 76.8% in CMM, significantly surpassing the baseline model’s accuracy of 34.5%. The SODA-14B model scored 95.1%, outperforming most commercial models, proving that specialized spatial cognition training enhances object control and path planning abilities.

Impact of Model Size Both the SODA-4B and SODA-14B models show advantages after training, especially in complex multi-turn tasks. SODA-14B excels with an accuracy of 99.8%, 97.3%, and 95.1% on DRM, SRM, and CMM tasks, respectively. The SODA-4B model still performs strongly in complex single-turn tasks (such as MPR and

DPR), with accuracies of 98.3% and 98.6%, surpassing many larger models. These results show that **SODA** enhances spatial reasoning in both large and small models.

Task-Level Performance Analysis Model performance varies across task levels. In Tier 1 (basic single-turn tasks), models showed high performance, with most exceeding 90%. As tasks became more complex in the Tier 2 (complex single-turn) and Tier 3 (multi-turn), model differences emerged. Non-reasoning models dropped significantly in performance with increased complexity. While most reasoning models performed better on harder tasks, some, like the grok 4.1, still declined in performance, highlighting the challenge of sustained reasoning over extended contexts.

4.3 Evaluating in SPACE

To demonstrate the generalizability of the **SODA**, we selected SPACE (Ramakrishnan et al., 2025) as an additional validation. SPACE encompasses multiple tasks, such as perspective taking and selective attention. The results in Table 3 show that, whether for SODA-4B or SODA-14B, both models performed excellently in most tasks, surpassing their base models, Qwen3-4B and Qwen3-14B,

Model	PTT_text	SAtt_text	CBTT_text	SAdd_text	MRT_text	MPFB_text	JLO_text
GPT-5	58.2	<u>99.0</u>	83.0	94.1	43.5	<u>51.0</u>	67.0
GPT-5 nano	51.5	94.8	58.0	61.2	31.0	35.5	30.5
o3	98.0	100.0	100.0	100.0	97.5	97.0	76.0
Qwen2.5-14B-Inst.	39.5	91.0	60.0	81.0	32.5	34.5	33.0
Qwen3-4B	97.0	100.0	76.0	96.5	58.8	31.5	59.5
Qwen3-14B	98.0	100.0	93.0	97.5	64.4	37.0	61.5
SODA-4B	<u>98.5</u>	100.0	84.0	<u>99.0</u>	70.0	37.5	63.5
SODA-14B	98.8	100.0	<u>96.0</u>	100.0	<u>76.3</u>	39.5	<u>68.5</u>

Table 3: Model performance (%) on the SPACE benchmark. Task abbreviations: DE = DirectionEstimation_BEVtext, DisE = DistanceEstimation_BEVtext, PTT = PerspectiveTaking_text, SA = SelectiveAttention_text, Corsi = CBTT_text, SAdd = SpatialAddition_text, MRT = MentalRotation_text, MS = MapSketching_BEVtext, MPFB = MPFB_text, JLO = JLO_text. “-” indicates the model was not evaluated on the corresponding task. The **best** and the second-best score in each column is shown in **bold** and underlined.

while also achieving comparable or superior performance to closed-source models, highlighting the advantage of SODA in spatial reasoning tasks.

4.4 Evaluation onto Reallife Application

4.4.1 Chess Combat

Model	Max Legal Moves	Min Legal Moves	Avg Legal Moves	Completion Rate (%)
<i>Baseline Models</i>				
GPT-5	22	2	8.50	5
Claude-3.7	6	0	2.46	0
Claude Opus 4.5	24	3	13.80	10
Deepseek-R1	21	0	6.60	0
Qwen3-4B	20	0	10.50	4
Qwen3-14B	26	1	13.50	12
o3	56	0	24.10	27
<i>Our Models</i>				
SODA-4B	28	<u>3</u>	14.87	86
SODA-14B	<u>35</u>	4	<u>16.01</u>	94

Table 4: Performance comparison on the Chess Combat task. Legal moves indicate the number of valid chess moves made during gameplay. Higher completion rates demonstrate better strategic understanding. The **best** and the second-best score in each column is shown in **bold** and underlined.

To evaluate the model’s generalization ability in complex spatial control tasks, we introduced chess combat, shown in Figure 4, as a test platform. This platform is based on chess rules and emphasizes coordination and confrontation among multiple pieces, requiring the model to integrate spatial perception, reasoning, and control. We used the Stockfish engine as the opponent and conducted 100 matches to assess the model’s average number of legal moves, completion rate, and maximum/minimum legal moves. As shown in Table 4, the results indicate that general-purpose large

language models perform poorly in chess combat, whereas the SODA models perform better. SODA-4B achieved 14.87 legal moves with an 86% completion rate, and SODA-14B further improved to 16.01 legal moves with a 94% completion rate, surpassing several closed-source systems. Without any specialized training, the SODA models successfully transferred to the chess task through spatial cognition training via OODA.

Error analysis revealed that LLMs struggle with board state awareness and adherence to chess rules, such as losing track of piece positions or violating fundamental rules. These errors collectively underscore the persistent gaps in long-range spatial tracking and rule-constrained planning.

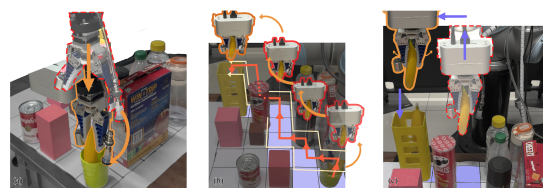


Figure 3: Robotic-arm Application: the model plans and executes obstacle-avoiding pick-and-place motions.

4.4.2 Embodied Validation on a Robotic Arm

To further assess the model’s capabilities and bridge the gap between abstract textual reasoning and embodied intelligence, we conducted experiments on a real robotic-arm platform, shown in Figure 3. The results demonstrate that the model can precisely control the arm to avoid obstacles and move target objects to their designated positions. More detailed content can be found in the appendix.

Model	Basic Single-Turn				Complex Single-Turn					Multi-Turn			
	OLD	SP	RD	MP	PS	MR	MPR	DPR	DR	DRM	SRM	MRM	CMM
SODA-4B(SFT only)	86.7	94.8	94.4	92.6	67.9	73.6	70.6	62.5	66.7	99.2	82.5	31.4	34.5
SODA-4B	99.5	82.1	97.3	88.9	100.0	93.6	98.3	98.6	46.7	60.3	59.4	31.4	76.8
SODA-14B(SFT only)	100.0	99.7	99.2	99.4	99.8	97.5	98.1	96.6	98.3	99.6	96.8	50.7	95.7
SODA-14B	100.0	97.6	99.8	99.3	100.0	98.2	100.0	100.0	95.1	99.8	97.3	63.9	95.1

Table 5: Ablation Results: SPOD-Bench performance (%) on SODA model(4B and 14B) after SFT and SFT-GRPO.

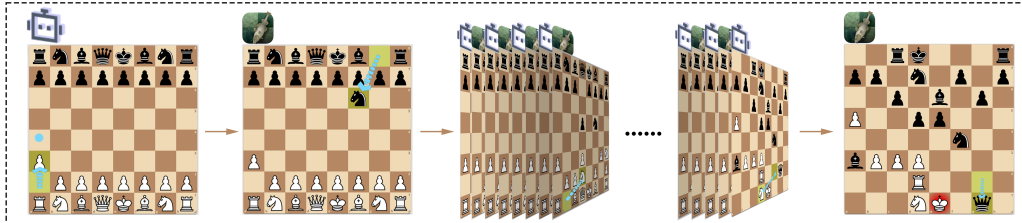


Figure 4: Chess Combat Evaluation & Application: an 8×8 grid-world chess setting that tests models’ integrated spatial perception, reasoning, and control against the Stockfish engine.

4.5 Sensitivity Analysis

Figure 5 shows the training dynamics of the **SODA** model during the GRPO stage. Whether for the 4B or 14B model, answer accuracy steadily improved after about 2,000 steps, with the 14B model converging faster and achieving higher final accuracy. This indicates that the GRPO strategy ensures stable optimization across different model sizes. Figure 5(b) shows that the average reward increased rapidly and synchronized with accuracy, staying consistently between -1.0 and 1.5, confirming that the dual-channel reward (answer correctness + OODA integrity) aligns with the task objectives and validating the stability of the reward strategy and the controllability of the training process. Figure 5(c) and (d) show that the token count for Observe and Orient rapidly increased during the first 1,000 steps and then saturated, while Decide and Act remained shorter. This suggests that the GRPO strategy helps the model prioritize allocating reasoning steps to perception and analysis, reducing redundant thinking and improving accuracy.

4.6 Ablation Experiment

The comparison between models using only SFT and the complete **SODA** framework highlights the effectiveness of the approach. As shown in the Table 5, the SODA-4B and SODA-14B models, combining SFT and GRPO, significantly outperform models using only SFT, especially in complex single-turn tasks and multi-turn tasks, with accuracy substantially improved. SODA-14B demonstrates high accuracy in basic tasks, complex tasks,

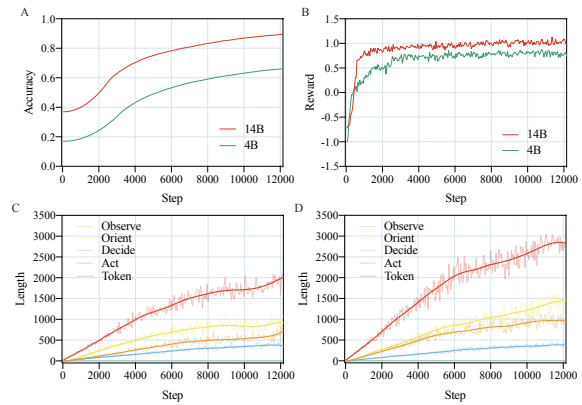


Figure 5: GRPO training curves

and multi-turn tasks, indicating that the full integration of the **SODA** training framework (SFT and GRPO) greatly enhances the model’s reasoning and spatial cognition capabilities.

5 Conclusion

This study presents **SODA**, a spatial-aware training framework that embeds the OODA reasoning mechanism into LLMs via two-stage training, using our conducted OODA-based dataset *SPOD-143k*. Additionally, we introduce *SPOD-Bench*, the first diverse and hierarchical pure-text spatial reasoning benchmark, covering tasks from perception to complex control and long-term planning. Results on both SPOD-bench and public datasets confirm that **SODA** not only outperforms its backbone models but also surpasses leading commercial models, also demonstrating its generalizations from strategic planning in chess to demonstrating its spatial control abilities through a real-world robot, offering new insights in a non-multimodal perspective.

6 Limitations

While this work offers a novel, non-multimodal perspective on enhancing the spatial capabilities of large language models (LLMs), our approach has several limitations. Our unimodal framework primarily provides insights into text-based spatial reasoning. However, the field is increasingly moving toward integrated systems that incorporate diverse sensory inputs to understand and interact with the world. To expand the model’s perceptual dimensions, future research should explore spatial understanding in other modalities, such as auditory perception from audio and visual perception from 2D, 3D, and 4D data. Building on the unimodal spatial-aware framework proposed in this paper, there is a clear need for more comprehensive and spatial-aware unified multimodal training strategies, which are crucial for developing the next generation of LLMs with physically-grounded understanding (Liu et al., 2025).

Additionally, while our model generalizes to existing benchmarks, its robustness in complex or Out-of-Distribution (OOD) scenarios requires further investigation. Current evaluation methods are limited in scope and lack comprehensive quantitative metrics. This necessitates next-generation benchmarks focused on quantitative reasoning (e.g., distance, size, angles) and dynamic transformations like motion. Dynamic reasoning, in particular, remains a significant challenge.

Finally, our exploration of real-world applications was limited. Future work can address application-level engineering, such as lightweight deployment and enhanced human-computer interaction. However, achieving true spatial intelligence will likely require fundamental shifts in training and architecture. Promising directions include joint multimodal pre-training and integrating components like persistent memory to build explicit, updatable world models.

References

Mark Abdollahian and Chasen Jeffries. 2024. Simulating boyd’s ooda loop: Towards an abm of human agency and sensemaking in dynamic, competitive environments. In *Proceedings of the 17th International Conference on Advances in Computer-Human Interactions (ACHI)*.

Josh Achiam, Steven Adler, Sandhini Agarwal, Lama Ahmad, Ilge Akkaya, Florencia Leoni Aleman, Diogo Almeida, Janko Altschmidt, Sam Altman,

Shyamal Anadkat, and 1 others. 2023. Gpt-4 technical report. *arXiv preprint arXiv:2303.08774*.

Mohamed Aghzal, Erion Plaku, and Ziyu Yao. 2025. Can large language models be good path planners? a benchmark and investigation on spatial-temporal reasoning. *Preprint*, arXiv:2310.03249.

Michael Ahn, Anthony Brohan, Noah Brown, Yevgen Chebotar, Omar Cortes, Byron David, Chelsea Finn, Chuyuan Fu, Keerthana Gopalakrishnan, Karol Hausman, and 1 others. 2022. Do as i can, not as i say: Grounding language in robotic affordances. *arXiv preprint arXiv:2204.01691*.

Anthropic. 2025. Claude 3: Next-generation capabilities for helpful and harmless language models. *arXiv preprint arXiv:2503.00001*, 1(1):1–45.

Anthropic. 2025. Introducing claude opus 4.5. <https://www.anthropic.com/news/claude-opus-4-5>.

Zechen Bai, Pichao Wang, Tianjun Xiao, Tong He, Zongbo Han, Zheng Zhang, and Mike Zheng Shou. 2025. Hallucination of multimodal large language models: A survey. *Preprint*, arXiv:2404.18930.

Mihir Bala, Aditya Chanana, Xiangliang Chen, Qifei Dong, Thomas Eiszler, Jingao Xu, Padmanabhan Pillai, and Mahadev Satyanarayanan. 2024. The ooda loop of cloudlet-based autonomous drones. In *2024 IEEE/ACM Symposium on Edge Computing (SEC)*, pages 178–190. IEEE.

Anant Bhatt and Amit Ganatra. 2022. Explosive weapons and arms detection with singular classification (wardic) on novel weapon dataset using deep learning: enhanced ooda loop. *Engineered Science*, 20(3):252–266.

Antonio Bollig, Marília Freire, Konrad Bücking, Jana Kühnapfel, and Markus Knaden. 2024. Aggressive conflict impacts path integration in homing desert ants. *bioRxiv*, pages 2024–11.

John R. Boyd. 1996. *The essence of winning and losing*. Unclassified briefing. Last version 28 June 1996.

Berndt Brehmer. 2005. The dynamic ooda loop: Amalgamating boyd’s ooda loop and the cybernetic approach to command and control. In *10th International Command and Control Research and Technology Symposium*, McLean, VA.

Anthony Brohan, Noah Brown, Justice Carbajal, Yevgen Chebotar, Xi Chen, Krzysztof Choromanski, Tianli Ding, Danny Driess, Avinava Dubey, Chelsea Finn, Pete Florence, Chuyuan Fu, Montse Gonzalez Arenas, Keerthana Gopalakrishnan, Kehang Han, Karol Hausman, Alexander Herzog, Jasmine Hsu, Brian Ichter, and 35 others. 2023. Rt-2: Vision-language-action models transfer web knowledge to robotic control. *Preprint*, arXiv:2307.15818.

608	Tom Brown, Benjamin Mann, Nick Ryder, Melanie	Joaquin M Fuster. 2004. Upper processing stages of the	662
609	Subbiah, Jared D Kaplan, Prafulla Dhariwal, Arvind	perception–action cycle. <i>Trends in cognitive sciences</i> ,	663
610	Neelakantan, Pranav Shyam, Girish Sastry, Amanda	8(4):143–145.	664
611	Askill, and 1 others. 2020. Language models are		
612	few-shot learners. <i>Advances in neural information</i>	Sean Gillies, Allan Doyle, Cal Smith Barber, and 1	665
613	<i>processing systems</i> , 33:1877–1901.	others. 2024. Shapely: Manipulation and analysis of	666
		geometric objects . Version 2.0.5.	667
614	Sébastien Bubeck, Varun Chandrasekaran, Ronen Eldan,	Daya Guo, Dejian Yang, Haowei Zhang, Junxiao Song,	668
615	Johannes Gehrke, Eric Horvitz, Ece Kamar, Peter	Peiyi Wang, Qihao Zhu, Runxin Xu, Ruoyu Zhang,	669
616	Lee, Yin Tat Lee, Yuanzhi Li, Scott Lundberg, and	Shirong Ma, Xiao Bi, Xiaokang Zhang, Xingkai Yu,	670
617	1 others. 2023. Sparks of artificial general intelli-	Yu Wu, Z. F. Wu, Zhibin Gou, Zhihong Shao, Zhu-	671
618	gence: Early experiments with gpt-4. <i>arXiv preprint</i>	oshu Li, Ziyi Gao, Aixin Liu, and 175 others. 2025.	672
619	<i>arXiv:2303.12712</i> .	Deepseek-r1 incentivizes reasoning in llms through	673
		reinforcement learning . <i>Nature</i> , 645(8081):633–638.	674
620	Cheng Chang, Siqi Wang, Jiawei Zhang, Jingwei Ge,		
621	and Li Li. 2024. Llmscenario: Large language	Aric A. Hagberg, Daniel A. Schult, Pieter J. Swart,	675
622	model driven scenario generation. <i>IEEE Transactions</i>	and the NetworkX Developers. 2025. NetworkX:	676
623	<i>on Systems, Man, and Cybernetics: Systems</i> ,	Network analysis in python. https://github.com/	677
624	54(11):6581–6594.	networkx/networkx . Version 3.5.	678
625	Boyuan Chen, Zhuo Xu, Sean Kirmani, Brian Ichter,	Dan Hendrycks, Collin Burns, Saurav Kadavath, Akul	679
626	Danny Driess, Pete Florence, Dorsa Sadigh, Leonidas	Arora, Steven Basart, Eric Tang, Dawn Song, and Ja-	680
627	Guibas, and Fei Xia. 2024. SpatialVLM: Endowing	cob Steinhardt. 2021. Measuring mathematical prob-	681
628	vision-language models with spatial reasoning capa-	lem solving with the math dataset. <i>arXiv preprint</i>	682
629	abilities . <i>Preprint</i> , arXiv:2401.12168.	<i>arXiv:2103.03874</i> .	683
630	Thomas Collett, Paul Graham, and Stanley Heinze.		
631	2025. The neuroethology of ant navigation . <i>Current</i>	Lei Huang, Weijiang Yu, Weitao Ma, Weihong Zhong,	684
632	<i>Biology</i> , 35(3):R110–R124.	Zhangyin Feng, Haotian Wang, Qianglong Chen,	685
633	DeepSeek-AI, Aixin Liu, Bei Feng, Bing Xue, Bingx-	Weihua Peng, Xiaocheng Feng, Bing Qin, and Ting	686
634	uan Wang, Bochao Wu, Chengda Lu, Chenggang	Liu. 2025. A survey on hallucination in large lan-	687
635	Zhao, Chengqi Deng, Chenyu Zhang, Chong Ruan,	guage models: Principles, taxonomy, challenges, and	688
636	Damai Dai, Daya Guo, Dejian Yang, Deli Chen,	open questions . <i>ACM Transactions on Information</i>	689
637	Dongjie Ji, Erhang Li, Fangyun Lin, Fucong Dai,	<i>Systems</i> , 43(2):1–55.	690
638	and 181 others. 2025. Deepseek-v3 technical report .		
639	<i>Preprint</i> , arXiv:2412.19437.	Zilong Ji, Eleonora Lomi, Kate Jeffery, Anna S Mitchell,	691
640	Ling L Dong and Ila R Fiete. 2024. Grid cells in cog-	and Neil Burgess. 2025. Phase precession relative to	692
641	gnition: mechanisms and function. <i>Annual Review of</i>	turning angle in theta-modulated head direction cells.	693
642	<i>Neuroscience</i> , 47.	<i>Hippocampus</i> , 35(2):e70008.	694
643	Danny Driess, Fei Xia, Mehdi SM Sajjadi, Corey Lynch,	Sangeet Khemlani, Tyler Tran, Nathaniel Gyory, An-	695
644	Aakanksha Chowdhery, Ayzaan Wahid, Jonathan	thony M. Harrison, Wallace E. Lawson, Ravenna	696
645	Tompson, Quan Vuong, Tianhe Yu, Wenlong Huang,	Thielstrom, Hunter Thompson, Taaren Singh, and	697
646	and 1 others. 2023. Palm-e: An embodied multi-	J. Gregory Trafton. 2025. Vision language models	698
647	modal language model.	are unreliable at trivial spatial cognition . <i>Preprint</i> ,	699
		arXiv:2504.16061.	700
648	Mengfei Du, Binhao Wu, Zejun Li, Xuanjing Huang,	Jing Yu Koh, Honglak Lee, Yinfei Yang, Jason	701
649	and Zhongyu Wei. 2024. Embspatial-bench: Bench-	Baldrige, and Peter Anderson. 2021. Pathdreamer:	702
650	marking spatial understanding for embodied tasks	A world model for indoor navigation . <i>Preprint</i> ,	703
651	with large vision-language models . <i>Preprint</i> ,	arXiv:2105.08756.	704
652	arXiv:2406.05756.		
653	Martin Egelhaaf and Jens P Lindemann. 2025. Path	Sang Ah Lee, Valeria A Sovrano, and Elizabeth S	705
654	integration and optic flow in flying insects: a review	Spelke. 2012. Navigation as a source of geomet-	706
655	of current evidence. <i>Journal of Comparative Physi-</i>	ric knowledge: Young children’s use of length, angle,	707
656	<i>ology A</i> , pages 1–27.	distance, and direction in a reorientation task. <i>Cogni-</i>	708
		<i>tion</i> , 123(1):144–161.	709
657	Robert E. Enck. 2012. The ooda loop . <i>Home Health</i>	Bohao Li, Yuying Ge, Yixiao Ge, Guangzhi Wang, Rui	710
658	<i>Care Management & Practice</i> , 24(3):123–124.	Wang, Ruimao Zhang, and Ying Shan. 2024. Seed-	711
659	Mica R Endsley. 2017. Toward a theory of situation	bench: Benchmarking multimodal large language	712
660	awareness in dynamic systems. In <i>Situational aware-</i>	models. In <i>Proceedings of the IEEE/CVF Conference</i>	713
661	<i>ness</i> , pages 9–42. Routledge.	<i>on Computer Vision and Pattern Recognition</i> , pages	714
		13299–13308.	715

716	Zhiqi Li, Wenhai Wang, Hongyang Li, Enze Xie, Chonghao Sima, Tong Lu, Qiao Yu, and Jifeng Dai. 2022. Bevformer: Learning bird’s-eye-view representation from multi-camera images via spatiotemporal transformers . <i>Preprint</i> , arXiv:2203.17270.	769
717		770
718		771
719		772
720		773
721	MingShan Liu and Jialing Fang. 2025. Enhancing mathematical reasoning in large language models with self-consistency-based hallucination detection . <i>Preprint</i> , arXiv:2504.09440.	774
722		775
723		776
724		
725	Weichen Liu, Qiyao Xue, Haoming Wang, Xiangyu Yin, Boyuan Yang, and Wei Gao. 2025. Spatial reasoning in multimodal large language models: A survey of tasks, benchmarks and methods . <i>Preprint</i> , arXiv:2511.15722.	777
726		778
727		779
728		780
729		781
730	Zoey Nguyen, Anthony Annunziata, Vinh Luong, Sang Dinh, Quynh Le, Anh Hai Ha, Chanh Le, Hong An Phan, Shruti Raghavan, and Christopher Nguyen. 2024. Enhancing qa with domain-specific fine-tuning and iterative reasoning: A comparative study . <i>Preprint</i> , arXiv:2404.11792.	782
731		783
732		784
733		785
734		786
735		787
736	OpenAI. 2023. Gpt-4 technical report . <i>arXiv preprint arXiv:2303.08774</i> , 1(1):1–60.	788
737		789
738	OpenAI. 2025. Introducing gpt-5 . https://openai.com/index/introducing-gpt-5/ .	790
739		791
740	Santhosh Kumar Ramakrishnan, Erik Wijmans, Philipp Kraehenbuehl, and Vladlen Koltun. 2025. Does spatial cognition emerge in frontier models? <i>Preprint</i> , arXiv:2410.06468.	792
741		793
742		794
743		795
744	Fedor Rodionov, Abdelrahman Eldesokey, Michael Birsak, John Femiani, Bernard Ghanem, and Peter Wonka. 2025. Planqa: A benchmark for spatial reasoning in llms using structured representations . <i>Preprint</i> , arXiv:2507.07644.	796
745		797
746		798
747		799
748		800
749	Zhihong Shao, Peiyi Wang, Qihao Zhu, Runxin Xu, Junxiao Song, Xiao Bi, Haowei Zhang, Mingchuan Zhang, Y. K. Li, Y. Wu, and Daya Guo. 2024. Deepseekmath: Pushing the limits of mathematical reasoning in open language models . <i>Preprint</i> , arXiv:2402.03300.	801
750		802
751		803
752		804
753		805
754		806
755	Dong Shu, Haiyan Zhao, Jingyu Hu, Weiru Liu, Ali Payani, Lu Cheng, and Mengnan Du. 2025. Large vision-language model alignment and misalignment: A survey through the lens of explainability . <i>Preprint</i> , arXiv:2501.01346.	807
756		808
757		809
758		810
759		811
760	Ilias Stogiannidis, Steven McDonagh, and Sotirios A. Tsaftaris. 2025. Mind the gap: Benchmarking spatial reasoning in vision-language models . <i>Preprint</i> , arXiv:2503.19707.	812
761		813
762		814
763		815
764	Dídac Surís, Sachit Menon, and Carl Vondrick. 2023. ViperGPT: Visual inference via python execution for reasoning . In <i>Proceedings of the IEEE/CVF international conference on computer vision</i> , pages 11888–11898.	816
765		817
766		818
767		819
768		820
		821
		822
	Susumu Takahashi, Fumiya Sawatani, Kaoru Ide, Takaaki K Abe, Takashi Kitagawa, and Yuya Makiguchi. 2024. Mapping spatial memory in teleosts: a new frontier in neural logging techniques . <i>Frontiers in Physiology</i> , 15:1499058.	
	Alexey Tikhonov. 2024. Plugh: A benchmark for spatial understanding and reasoning in large language models . <i>Preprint</i> , arXiv:2408.04648.	
	Jiayu Wang, Yifei Ming, Zhenmei Shi, Vibhav Vineet, Xin Wang, Yixuan Li, and Neel Joshi. 2024. Is a picture worth a thousand words? delving into spatial reasoning for vision language models . <i>Preprint</i> , arXiv:2406.14852.	
	Wenshan Wu, Shaoguang Mao, Yadong Zhang, Yan Xia, Li Dong, Lei Cui, and Furu Wei. 2024. Mind’s eye of llms: visualization-of-thought elicits spatial reasoning in large language models . <i>Advances in Neural Information Processing Systems</i> , 37:90277–90317.	
	xAI. 2025. Grok 4.1 . https://x.ai/news/grok-4-1 .	
	Zikai Xie. 2025. Order matters in hallucination: Reasoning order as benchmark and reflexive prompting for large-language-models . <i>Preprint</i> , arXiv:2408.05093.	
	Liuchang Xu, Shuo Zhao, Qingming Lin, Luyao Chen, Qianqian Luo, Sensen Wu, Xinyue Ye, Hailin Feng, and Zhenhong Du. 2024. Evaluating large language models on spatial tasks: A multi-task benchmarking study . <i>arXiv preprint arXiv:2408.14438</i> .	
	Li Xuan, Zhang Haoxiang, Jiang Baozheng, Li Yanxia, and Li You. 2024. A benchmark dataset for evaluating spatial perception in multimodal large models . In <i>Proceedings of the First International Workshop on IoT Datasets for Multi-modal Large Model</i> , pages 37–43.	
	Yutaro Yamada, Yihan Bao, Andrew K. Lampinen, Jungo Kasai, and Ilker Yildirim. 2024. Evaluating spatial understanding of large language models . <i>Preprint</i> , arXiv:2310.14540.	
	An Yang, Anfeng Li, Baosong Yang, Beichen Zhang, Binyuan Hui, Bo Zheng, Bowen Yu, Chang Gao, Chengen Huang, Chenxu Lv, Chujie Zheng, Dayiheng Liu, Fan Zhou, Fei Huang, Feng Hu, Hao Ge, Haoran Wei, Huan Lin, Jialong Tang, and 41 others. 2025. Qwen3 technical report . <i>Preprint</i> , arXiv:2505.09388.	
	Xiaoli Yang and Yuejuan Pan. 2021. Spatial language of young children during block play in kindergartens in urban china . <i>Frontiers in Psychology</i> , 12:568638.	
	Zhiyu Yin, Kehai Chen, Xuefeng Bai, Ruili Jiang, Juntao Li, Hongdong Li, Jin Liu, Yang Xiang, Jun Yu, and Min Zhang. 2025. A survey: Spatiotemporal consistency in video generation . <i>Preprint</i> , arXiv:2502.17863.	

823
824
825
826
827
828
829
830
831
832
833
834
835
836
837
838
839
840
841
842
843
844
845
846
847
848
849
850
851
852
853
854
855
856
857
858
859
860
861
862
863
864
865
866
867
868
869
870
871
872
873

A Appendix

B Datasets and Conversation Examples

Tier 1 (Basic Single-Turn Tasks):

memory_path(MP):

A similar paradigm was introduced by Mittelstaedt et al. while investigating the path-integration mechanism that supports homing behavior in rodents. Gerbils had to correctly account for spatial changes caused by translations or rotations of the arena. In recent years, several reading-comprehension and large-language-model benchmarks have required models to handle analogous position-update mechanisms (Weston et al., 2016).

In our implementation, we randomly sample a starting point (x_0, y_0) and then generate an action sequence of 5–15 moves drawn from (N, S, E, W), with each move shifting the position by ± 1 unit. The sequence is constructed so that it uniquely determines an end point. The model must compute $\Sigma(\Delta x, \Delta y)$ and return the final coordinates.

Conversation Examples:

memory_path(MP):

Q: Starting coordinates (1, 1), follow the action sequence W E N S W E N W S N to walk; which option below is the final

coordinate? Please select and answer only the letter: A:(1, 3); B:(2, 0); C:(0, 2); D:(8, 8)

A:C

object_location_distance (OLD):

A distance-estimation task. This type of exercise dates back to the foundations of analytic geometry, where points are expressed in coordinates and the Pythagorean theorem is used to compute the distance between two points, establishing the methodological basis for later “coordinate-distance” drills. In contemporary psychology and neuroscience, the task is regarded as a classic paradigm for assessing metric spatial representations, used to test the accuracy with which cognitive maps encode distances (Shepard, 1987).

Our implementation randomly generates the coordinates of two points. Given these coordinates, the model must calculate the Euclidean distance between the two points.

Conversation Examples:

object_location_distance:

Q: The position of object A is (3.44, 8.17), and the position of object B is (6.72, 7.32). Which option

below is closest to the Euclidean distance between them? Please select and answer only the letter: A:3.48; B:3.38; C:2.19; D:4.73

A:B

relative_direction (RD):

This task falls under “relative direction–distance estimation.” It simultaneously tests the ability to represent discrete directions and continuous distances, and is commonly used to assess two-dimensional geometric reasoning and numerical-approximation skills in humans or large language models. Relative-direction training is also employed in the computational cognitive model of direction judgments by Phillip M. Newman et al.

Our implementation randomly provides reasonable coordinates for two points A and B; the model must judge which of the eight compass sectors (N/NE/E/SE/S/SW/W/NW) point B occupies relative to point A, then compute the Euclidean distance, and finally select, from several options, the combination closest to the correct answer.

Conversation Examples:

relative_direction:

Q: The coordinates of object A are (8.50, 2.60), and the coordinates of object B are (0.74, 5.94). Which option most accurately describes the direction and distance of B relative to A? Please select and answer only the letter: A:Direction: NE; Distance: 5.14 units; B:Direction: S; Distance: 5.69 units; C:Direction: W; Distance: 10.15 units; D:Direction: NW; Distance: 8.45 units

A:D

shortest_path (SP):

This task resembles the traveling salesman problem (TSP) task, discussed in detail by MacGregor and Ormerod (1996), and is used in laboratory settings to test graph-based spatial problem solving. Participants see on paper a lattice layout of 10 or 20 points and must freely choose a starting point, draw the shortest closed path that visits all points and returns to the start, and clearly mark both the starting point and the travel direction; the solution is presented as a hand-drawn path. In recent years, this task has been used to evaluate the graph-navigation performance of large neural networks capable of learning structured representations (Kool et al., 2018). Our implementation randomly generates an undirected graph with 5–15 nodes and an unequal number of edges, randomly

874
875
876
877
878
879
880
881
882
883
884
885
886
887
888
889
890
891
892
893
894
895
896
897
898
899
900
901
902
903
904
905
906
907
908
909
910
911
912
913
914
915
916
917
918
919
920
921
922
923
924
925

926 selects distinct start and end points, and requires
927 computation of the unique shortest path.

928
929 Conversation Examples:

930 **shortest_path:**

931 Q:Given an undirected graph, the node set is
932 ['A', 'B', 'C', 'D', 'E', 'F', 'G'], and the edge
933 set is {A-D, A-F, B-C, B-D, B-E, B-G}. Write
934 the shortest path from node E to node A. Which
935 option below is the shortest path? Please select and
936 answer only the letter: A:E-D-A-B; B:E-B-D-A;
937 C:B-D-E-A; D:E-A-B-D
938 A:B
939

940 **B.0.1 Tier 2(Complex Single-Turn Tasks):**

941 **packing_shapes (PS):**

942 Okagaki and Frensch proposed a similar problem;
943 it is a computerized, two-dimensional bin-packing
944 task used to study the acquisition of visuo-spatial
945 skills and strategic planning. In this task, partici-
946 pants train mental rotation and visualization skills
947 with Tetris-like stimuli: the screen displays a fixed-
948 size rectangular “container” together with several
949 geometric shapes, and participants must translate
950 and rotate all shapes to fit them into the container
951 while minimizing unused blank area. This
952 paradigm has recently served as a spatial-reasoning
953 benchmark for deep-reinforcement-learning
954 agents learning packing strategies (Wang et al.,
955 2022). Our implementation randomly generates
956 a rectangular plane of reasonable, random size
957 and simultaneously generates five rectangles and
958 circles that can fit inside the plane, then instructs
959 the model to compute the remaining blank area.
960

961 Conversation Examples:

962 **packing_shapes:**

963 Q:Given a 9.43×9.62 rectangular packing area,
964 and the following objects: Object 1: Rectangle,
965 width 2.72, height 2.88; Object 2: Rectangle, width
966 1.19, height 1.74; Object 3: Rectangle, width 2.33,
967 height 1.64; Object 4: Circle, radius 1.08; Object 5:
968 Circle, radius 1.78. Which option below is closest
969 to the correct remaining space? Please select and
970 answer only the letter: A: Remaining space: 64.30
971 square units; B: Remaining space: 72.95 square
972 units; C: Remaining space: 63.32 square units; D:
973 Remaining space: 54.15 square units.
974 A:C
975

976 **mental_rotation (MR):**

This paradigm originates from Shepard & Met-
zler’s (1971) pioneering study on matching rotated
3-D objects and was quantified by Cooper &
Shepard (1973) as the classic effect wherein
reaction time increases linearly with rotation angle
 θ . In our task, the model must apply a specified
axis rotation to an object’s orientation vector held
in working memory, then judge which option
among several best matches the resulting vector.
The task assesses abilities in 3-D coordinate
transformation, spatial orientation updating, and
mental-rotation speed.

988 Conversation Examples:

989 **mental_rotation:**

990 Q:The forward vector of a cube is (1, 0, 0). It
991 is rotated counterclockwise by 274° around the
992 axis vector (-0.599, +0.289, +0.746). Which of
993 the following is the forward vector after rotation?
994 Please select and answer only the letter: A:(-0.641,
995 +0.244, -0.728); B:(+0.041, +0.054, +0.998);
996 C:(+0.404, -0.906, -0.128); D:(+0.113, +0.296,
997 -0.948).
998 A:C
999

1000
1001 **Doublepoint-relation Test (DPR) & Multipoint-**
1002 **relation Test (MPR):**

1003 This paradigm is adapted from the original
1004 “multi-segment direction-distance reasoning” task
1005 used to study human way-finding and cartographic
1006 cognition (Kozhevnikov et al., 2001). In the test,
1007 participants are shown a 2-D array of objects,
1008 imagine adopting a perspective within the array,
1009 and indicate the direction of a target object from
1010 that viewpoint. In recent years it has also been
1011 adapted to evaluate large-language-model (LLM)
1012 spatial-reasoning ability (Danish et al., 2024).
1013 Unlike the classical test, the MPR is entirely text-
1014 based and leverages the model’s computational
1015 capacity, making it easy to administer to language
1016 models.
1017

1018 Our implementation is as follows:

1019 •**Doublepoint-relation Test:** randomly generate
1020 two geographic coordinates within a fixed range;
1021 the model must compute the geographic distance
1022 between the two points and infer their precise
1023 spatial relation.

1024 •**Multipoint-relation Test:** take an arbitrary seed
1025 coordinate as the center, randomly sample four real
1026 POIs within a given radius, and provide the spatial
1027 and distance relations $POI_1 \rightarrow POI_2$, $POI_2 \rightarrow$
1028 POI_3 , $POI_3 \rightarrow POI_4$; the model must infer the

1029	composite relation $POI_1 \rightarrow POI_4$.	
1030	Conversation Examples:	
1031	doublepoint_relation:	
1032	Q:Coordinates A(120.030685,30.246885), and	
1033	B(120.317380,30.404990).Which option most	
1034	reliably describes the direction and distance	
1035	of B relative to A? Please select and answer	
1036	only the letter: A:Direction: N86.2°E; Distance:	
1037	28.4 km; B:Direction: N61.1°E; Distance: 32.7	
1038	km; C:Direction: N63.7°E; Distance: 24.0 km;	
1039	D:Direction: N31.9°E; Distance: 27.5 km.	
1040	A:B	
1041		
1042	multiptoint_relation:	
1043	Q:Zhejiang Deren Financial Co., Ltd. is located	
1044	1.5 km south-southeast (19.2°) of Xinghuo	
1045	Apartment Building 2. Xinghuo Apartment	
1046	Building 2 is 27.1 km south-southeast (83.0°) of	
1047	Hangda Equipment. Hangda Equipment is 19.4	
1048	km south-southwest (48.3°) of Chengdong Primary	
1049	School (Bus Stop). What is the direction and	
1050	distance from A to D? Please select and answer	
1051	only the letter: A:Direction: S22.3°E; Distance:	
1052	27.9 km; B:Direction: S15.3°E; Distance: 30.4	
1053	km; C:Direction: S36.1°E; Distance: 21.9 km;	
1054	D:Direction: S41.8°E; Distance: 24.8 km.	
1055	A:C	
1056		
1057	door_rotation(DR):	
1058	Circular–orientation updating task (COU):	
1059	This paradigm stems from research on human	
1060	self-motion heading maintenance. Wang & Spelke	
1061	(2000) showed that, in enclosed spaces, individuals	
1062	can rely on a “post-rotation updating” mechanism	
1063	to maintain an instantaneous representation	
1064	of a target’s direction. The task is a circular	
1065	viewpoint-updating paradigm inspired by studies	
1066	on self-motion and heading maintenance, espe-	
1067	cially the spatial-updating model for self-rotation	
1068	in closed environments proposed by Wang et al.	
1069	(2000), which has informed cognitive psychology.	
1070	Our implementation presents, in verbal form,	
1071	an experimental scene with a circular array of	
1072	randomly segmented, sequentially colored door	
1073	panels. The initial target is hidden behind the	
1074	first door directly in front of the model;then the	
1075	sytem rotates the model environment. the model	
1076	must rely on memory to track its own orientation	
1077	changes and continuously infer the current index	
1078	of the target door.	
1079		
1080	Conversation Examples:	
	door_rotation:	1081
	Q:You are currently at a 9-door hub with doors	1082
	surrounding you. Target A is behind the door	1083
	directly in front of you. The colors of the 9	1084
	doors (starting directly in front of you and going	1085
	clockwise) are: Cyan, Red, Orange, Red, Blue,	1086
	Blue, Cyan, Orange, Green. Then, you are rotated	1087
	counterclockwise by 3 doors (shifted 3 positions	1088
	left). The new colors of the doors starting directly	1089
	in front of you and going clockwise are: Red, Blue,	1090
	Blue, Cyan, Orange, Green, Cyan, Red, Orange.	1091
	Which door is Target A now behind? Please select	1092
	one option and answer only the letter: A: Door 5;	1093
	B: Door 2; C: Door 4; D: Door 6.	1094
	A:C	1095
		1096
	B.0.2 Tier 3	1097
	door_rotation_multiturn(DRM):	1098
	Based on the previous door_rotation(DR) method,	1099
	the difference is that in the door_rotation_multiturn	1100
	task the environment is rotated multiple times,	1101
	and the model must rely on memory to track its	1102
	own orientation changes and infer the target door’s	1103
	number in real time.	1104
		1105
	Conversation Examples:	1106
	door_rotation_multiturn:	1107
	Q:In a circular space with 13 doors, each door has	1108
	a unique color. Target A is behind the 1st door	1109
	directly in front of you. The colors of the doors	1110
	clockwise from your position are: Orange, Black,	1111
	Blue, Red, Orange, Purple, Blue, Brown, Black,	1112
	Green, White, Cyan, Yellow. After being rotated,	1113
	the new colors clockwise from your position	1114
	are: White, Cyan, Yellow, Orange, Black, Blue,	1115
	Red, Orange, Purple, Blue, Brown, Black, Green.	1116
	Where is Target A now? A. Door 7 B. Door 4 C.	1117
	Door 5 D. Door 10.	1118
	A:B	1119
	Q:You were rotated again. After the rotation,	1120
	the new colors clockwise from your position are:	1121
	Black, Green, White, Cyan, Yellow, Orange, Black,	1122
	Blue, Red, Orange, Purple, Blue, Brown. Where is	1123
	Target A now? A. Door 2 B. Door 6 C. Door 13 D.	1124
	Door 5	1125
	A:B	1126
	Q:You were rotated again. After the rotation,	1127
	the new colors clockwise from your position are:	1128
	Yellow, Orange, Black, Blue, Red, Orange, Purple,	1129
	Blue, Brown, Black, Green, White, Cyan. Where	1130
	is Target A now? A. Door 6 B. Door 2 C. Door 11	1131

1132	D. Door 5.	spatial_relation_multiturn(SRM):	1184
1133	A:B	Based on the aforementioned relative-direction	1185
1134	Q:You were rotated again. After the rotation,	approach, we introduce multi-turn dialogue	1186
1135	the new colors clockwise from your position are:	operations to increase training complexity and	1187
1136	Blue, Brown, Black, Green, White, Cyan, Yellow,	enhance the model's ability to comprehensively	1188
1137	Orange, Black, Blue, Red, Orange, Purple. Where	retain key contextual information.	1189
1138	is Target A now? A. Door 4 B. Door 3 C. Door 8		1190
1139	D. Door 10	Conversation Examples:	1191
1140	A:C	spatial_relation_multiturn: Q:The coordinates	1192
1141	Q:You were rotated again. After the rotation,	of object A are (40.77, 31.69). Object B is located	1193
1142	the new colors clockwise from your position are:	SW of object A at a distance of 9.61 units. What	1194
1143	Orange, Black, Blue, Red, Orange, Purple, Blue,	is the direction and distance of object B relative	1195
1144	Brown, Black, Green, White, Cyan, Yellow. Where	to object A? A: Direction: W; Distance: 13.27	1196
1145	is Target A now? A. Door 1 B. Door 7 C. Door 6	units B: Direction: NE; Distance: 10.50 units C:	1197
1146	D. Door 9	Direction: SW; Distance: 9.61 units D: Direction:	1198
1147	A:A	E; Distance: 9.61 units A:C Q:The coordinates of	1199
1148	Q:You were rotated again. After the rotation,	object A are (40.77, 31.69). Object C is located	1200
1149	the new colors clockwise from your position are:	NE of object B at a distance of 9.72 units. What	1201
1150	Orange, Black, Blue, Red, Orange, Purple, Blue,	is the direction and distance of object C relative	1202
1151	Brown, Black, Green, White, Cyan, Yellow. Where	to object A? A: Direction: NE; Distance: 0.10	1203
1152	is Target A now? A. Door 4 B. Door 1 C. Door 10	units B: Direction: SE; Distance: 0.12 units C:	1204
1153	D. Door 5	Direction: E; Distance: 0.10 units D: Direction:	1205
1154	A:B	W; Distance: 0.08 units A:A Q:The coordinates of	1206
1155	Q:You were rotated again. After the rotation,	object A are (40.77, 31.69). Object D is located	1207
1156	the new colors clockwise from your position are:	SW of object C at a distance of 3.10 units. What	1208
1157	Black, Blue, Red, Orange, Purple, Blue, Brown,	is the direction and distance of object D relative	1209
1158	Black, Green, White, Cyan, Yellow, Orange.	to object A? A: Direction: SW; Distance: 3.00	1210
1159	Where is Target A now? A. Door 8 B. Door 13 C.	units B: Direction: E; Distance: 1.82 units C:	1211
1160	Door 1 D. Door 11	Direction: N; Distance: 3.76 units D: Direction:	1212
1161	A:B	SE; Distance: 2.70 units A:A Q:The coordinates of	1213
1162	Q:You were rotated again. After the rotation,	object A are (40.77, 31.69). Object E is located	1214
1163	the new colors clockwise from your position are:	S of object D at a distance of 6.03 units. What	1215
1164	Black, Green, White, Cyan, Yellow, Orange, Black,	is the direction and distance of object E relative	1216
1165	Blue, Red, Orange, Purple, Blue, Brown. Where is	to object A? A: Direction: E; Distance: 11.31	1217
1166	Target A now? A. Door 13 B. Door 11 C. Door 6	units B: Direction: SW; Distance: 6.61 units C:	1218
1167	D. Door 2	Direction: NW; Distance: 6.53 units D: Direction:	1219
1168	A:C	S; Distance: 8.42 units A:D Q:The coordinates of	1220
1169	Q:You were rotated again. After the rotation,	object A are (40.77, 31.69). Object F is located	1221
1170	the new colors clockwise from your position are:	NW of object E at a distance of 6.77 units. What	1222
1171	Black, Blue, Red, Orange, Purple, Blue, Brown,	is the direction and distance of object F relative	1223
1172	Black, Green, White, Cyan, Yellow, Orange.	to object A? A: Direction: N; Distance: 9.47	1224
1173	Where is Target A now? A. Door 11 B. Door 13 C.	units B: Direction: NE; Distance: 8.71 units C:	1225
1174	Door 7 D. Door 3	Direction: NW; Distance: 4.89 units D: Direction:	1226
1175	A:B	SW; Distance: 7.68 units A:D Q:The coordinates	1227
1176	Q:You were rotated again. After the rotation,	of object A are (40.77, 31.69). Object G is located	1228
1177	the new colors clockwise from your position are:	SW of object F at a distance of 8.10 units. What	1229
1178	Cyan, Yellow, Orange, Black, Blue, Red, Orange,	is the direction and distance of object G relative	1230
1179	Purple, Blue, Brown, Black, Green, White. Where	to object A? A: Direction: W; Distance: 11.24	1231
1180	is Target A now? A. Door 3 B. Door 12 C. Door 1	units B: Direction: SW; Distance: 15.57 units C:	1232
1181	D. Door 13	Direction: NE; Distance: 12.62 units D: Direction:	1233
1182	A:A	SE; Distance: 15.37 units A:B Q:The coordinates	1234
1183		of object A are (40.77, 31.69). Object H is located	1235

1236	NW of object G at a distance of 4.96 units. What	clockwise from 0°, where 0° indicates right, 90°	1288
1237	is the direction and distance of object H relative	down, 180° left, and 270° up. The object moves	1289
1238	to object A? A: Direction: N; Distance: 11.81	0.9 units in the direction of 73°. What is the	1290
1239	units B: Direction: E; Distance: 17.73 units C:	object's new position? A. (1,7) B. (0,7) C. (1,6) D.	1291
1240	Direction: W; Distance: 17.08 units D: Direction:	(1,8)	1292
1241	NE; Distance: 20.00 units A:C Q:The coordinates	A:C	1293
1242	of object A are (40.77, 31.69). Object I is located	Q:After moving 0.9 units in the direction of	1294
1243	NE of object H at a distance of 2.43 units. What	73°, the object continues to move 3.7 units in	1295
1244	is the direction and distance of object I relative	the direction of 146°. What is the object's new	1296
1245	to object A? A: Direction: S; Distance: 17.98	position? A. (1,7) B. (0,7) C. (1,8) D. (0,8)	1297
1246	units B: Direction: W; Distance: 14.94 units C:	A:D	1298
1247	Direction: E; Distance: 16.63 units D: Direction:	Q:After moving 3.7 units in the direction of	1299
1248	NW; Distance: 14.81 units A:B Q:The coordinates	146°, the object continues to move 2.3 units in	1300
1249	of object A are (40.77, 31.69). Object J is located	the direction of 343°. What is the object's new	1301
1250	S of object I at a distance of 7.81 units. What	position? A. (4,7) B. (3,6) C. (2,6) D. (2,7)	1302
1251	is the direction and distance of object J relative	A:D	1303
1252	to object A? A: Direction: SW; Distance: 18.56	Q:After moving 2.3 units in the direction of	1304
1253	units B: Direction: S; Distance: 14.85 units C:	343°, the object continues to move 3.9 units in	1305
1254	Direction: N; Distance: 20.61 units D: Direction:	the direction of 217°. What is the object's new	1306
1255	W; Distance: 21.46 units A:A Q:The coordinates	position? A. (0,4) B. (1,6) C. (0,3) D. (0,5)	1307
1256	of object A are (40.77, 31.69). Object K is located	A:D	1308
1257	SW of object J at a distance of 2.59 units. What	Q:After moving 3.9 units in the direction of	1309
1258	is the direction and distance of object K relative	217°, the object continues to move 1.3 units in	1310
1259	to object A? A: Direction: W; Distance: 23.38	the direction of 328°. What is the object's new	1311
1260	units B: Direction: S; Distance: 15.30 units C:	position? A. (2,5) B. (0,3) C. (1,5) D. (1,4)	1312
1261	Direction: E; Distance: 15.77 units D: Direction:	A:D	1313
1262	SW; Distance: 21.14 units A:D	Q:After moving 1.3 units in the direction of	1314
1263	coordinates_movement_multiturn(CMM):	328°, the object continues to move 1.0 unit in	1315
1264	This task is a two-dimensional "path-integration"	the direction of 341°. What is the object's new	1316
1265	coordinate-updating problem, reminiscent of the	position? A. (2,6) B. (2,3) C. (2,4) D. (1,3) A:C	1317
1266	classic account of animal path integration by	Q:After moving 1.0 unit in the direction of 341°,	1318
1267	Mittelstaedt et al. (1980).	the object continues to move 0.8 units in the	1319
1268	Within a 9 × 9 integer grid, the system successively	direction of 1°. What is the object's new position?	1320
1269	issues movement commands expressed in clock-	A. (4,3) B. (3,3) C. (3,4) D. (4,4)	1321
1270	wise bearings with magnitudes (e.g., 73°, 146°).	A:C	1322
1271	After each command, the participant must instantly	Q:After moving 0.8 units in the direction of 1°, the	1323
1272	convert the polar displacement into Cartesian	object continues to move 4.6 units in the direction	1324
1273	offsets, add them to the current floating-point	of 285°. What is the object's new position? A.	1325
1274	position, and report the object's new coordinates.	(4,2) B. (2,0) C. (6,0) D. (4,0)	1326
1275	The system verifies the answer before providing	A:D	1327
1276	the next instruction, and accuracy is assessed only	Q:After moving 4.6 units in the direction of	1328
1277	after the final move.	285°, the object continues to move 2.0 units in	1329
1278	The task primarily tests the subject's real-time	the direction of 248°. What is the object's new	1330
1279	vector decomposition and planar-geometry	position? A. (3,1) B. (5,0) C. (1,0) D. (3,0)	1331
1280	computation skills, as well as the ability to keep	A:D	1332
1281	cumulative error to a minimum over multiple	Q:After moving 2.0 units in the direction of	1333
1282	dialogue turns.	248°, the object continues to move 4.1 units in	1334
1283		the direction of 351°. What is the object's new	1335
1284	Conversation Examples:	position? A. (7,0) B. (5,0) C. (7,1) D. (6,0)	1336
1285	coordinates_movement_multiturn:	A:A	1337
1286	Q:In a 9x9 grid (coordinates ranging from 0 to		1338
1287	8), an object starts at (1,5). Angles are measured	mental_rotation_multiturn (MRM):	1339

1340	This task is a continuous, interactive three-	(-0.307, -0.594, 0.744); B: (0.919, 0.332, 0.212); C:	1392
1341	dimensional mental-rotation assessment:The	(0.844, -0.155, 0.513); D: (0.620, -0.784, 0.049).	1393
1342	system sequentially issues counter-clockwise	A:D	1394
1343	rotation angles about arbitrary unit vectors.After	Q:After being rotated counterclockwise 265°	1395
1344	each command, the participant must compute the	around the axis (-0.070, -0.834, -0.548), the cube	1396
1345	new, compounded forward vector based on the	continues to rotate counterclockwise 52° around	1397
1346	previous orientation and select a single answer	the axis (0.632, -0.688, 0.355). Which of the	1398
1347	from options A, B, C, or D.The system confirms	following is the forward vector after rotation?	1399
1348	the response, then delivers the next rotation. After	Please select and respond with the letter only: A:	1400
1349	the final step, overall accuracy is evaluated.	(0.823, -0.364, 0.437); B: (0.148, -0.295, 0.944);	1401
1350	The test traces its theoretical roots to the mental-	C: (0.805, -0.585, 0.105); D: (0.179, 0.324, 0.929).	1402
1351	rotation experiment introduced by Shepard et al.	A:C	1403
1352	in 1971. Modern computational implementations	Q:After being rotated counterclockwise 52° around	1404
1353	generally draw on Zacks' (2008) review of	the axis (0.632, -0.688, 0.355), the cube continues	1405
1354	the cognitive mechanisms underlying rotation,	to rotate counterclockwise 114° around the axis	1406
1355	ensuring that the task's algorithmic and cognitive	(0.658, 0.633, 0.408). Which of the following is	1407
1356	demands remain aligned.	the forward vector after rotation? Please select	1408
1357		and respond with the letter only: A: (0.139, 0.655,	1409
1358	Conversation Examples:	-0.744); B: (-0.754, 0.432, 0.494); C: (-0.836,	1410
1359	mental_rotation_multiturn:	-0.303, 0.457); D: (0.028, -0.370, 0.929).	1411
1360	Q:A cube's initial forward vector is (1.000, 0.000,	A:A	1412
1361	0.000). It is rotated counterclockwise 205° around	Q:After being rotated counterclockwise 114°	1413
1362	the axis (-0.943, -0.307, 0.128). Which of the	around the axis (0.658, 0.633, 0.408), the cube	1414
1363	following is the forward vector after rotation?	continues to rotate counterclockwise 201° around	1415
1364	Please select and respond with the letter only: A:	the axis (-0.474, 0.202, -0.857). Which of the	1416
1365	(0.790, 0.498, -0.359); B: (0.553, 0.650, 0.520); C:	following is the forward vector after rotation?	1417
1366	(0.103, 0.010, 0.995); D: (-0.119, 0.352, 0.928).	Please select and respond with the letter only: A:	1418
1367	A:A	(-0.125, -0.195, 0.973); B: (-0.922, -0.168, -0.351);	1419
1368	Q:After being rotated counterclockwise 205°	C: (0.878, -0.465, -0.110); D: (-0.844, -0.524,	1420
1369	around the axis (-0.943, -0.307, 0.128), the cube	0.117).	1421
1370	continues to rotate counterclockwise 286° around	A:B	1422
1371	the axis (0.105, -0.718, -0.688). Which of the	Q:After being rotated counterclockwise 201°	1423
1372	following is the forward vector after rotation?	around the axis (-0.474, 0.202, -0.857), the cube	1424
1373	Please select and respond with the letter only: A:	continues to rotate counterclockwise 125° around	1425
1374	(-0.362, 0.638, -0.680); B: (0.896, 0.331, 0.297); C:	the axis (-0.117, -0.936, 0.331). Which of the	1426
1375	(0.501, -0.828, -0.251); D: (-0.849, -0.517, 0.109).	following is the forward vector after rotation?	1427
1376	A:A	Please select and respond with the letter only: A:	1428
1377	Q:After being rotated counterclockwise 286°	(-0.734, 0.085, -0.674); B: (0.816, -0.407, -0.412);	1429
1378	around the axis (0.105, -0.718, -0.688), the cube	C: (0.182, -0.875, -0.449); D: (-0.897, 0.294,	1430
1379	continues to rotate counterclockwise 240° around	-0.330).	1431
1380	the axis (0.733, -0.433, -0.525). Which of the	A:B	1432
1381	following is the forward vector after rotation?	Q:After being rotated counterclockwise 125°	1433
1382	Please select and respond with the letter only: A:	around the axis (-0.117, -0.936, 0.331), the cube	1434
1383	(-0.316, 0.448, 0.836); B: (-0.667, 0.278, 0.691); C:	continues to rotate counterclockwise 233° around	1435
1384	(-0.603, -0.283, 0.746); D: (-0.567, -0.795, 0.217).	the axis (0.254, 0.947, -0.195). Which of the	1436
1385	A:D	following is the forward vector after rotation?	1437
1386	Q:After being rotated counterclockwise 240°	Please select and respond with the letter only: A:	1438
1387	around the axis (0.733, -0.433, -0.525), the cube	(0.941, -0.224, -0.254); B: (0.140, 0.718, 0.682); C:	1439
1388	continues to rotate counterclockwise 265° around	(-0.365, -0.756, -0.544); D: (-0.156, 0.140, 0.978).	1440
1389	the axis (-0.070, -0.834, -0.548). Which of the	A:D	1441
1390	following is the forward vector after rotation?	Q:After being rotated counterclockwise 233°	1442
1391	Please select and respond with the letter only: A:	around the axis (0.254, 0.947, -0.195), the cube	1443

1444	continues to rotate counterclockwise 274° around the axis $(-0.951, 0.174, 0.256)$. Which of the following is the forward vector after rotation? Please select and respond with the letter only: A: $(-0.890, -0.361, -0.279)$; B: $(0.855, -0.344, 0.388)$; C: $(0.995, 0.059, -0.084)$; D: $(-0.519, -0.810, 0.274)$.	Output step by step.	1495
1445	A:D	A:NW	1496
1446		Q:Step 1 executed. Continue.	1497
1447		1498
1448		Q:Step n executed. Continue.	1499
1449		A:NONE.Action sequence: NW, NW, N	1500
1450			1501
1451		single_free_obstacle_path_planning_9_multiturn:	1502
1452		Q:Task: 9×9 grid, move from (7, 6) to (2, 1). Output step by step.	1503
1453	B.0.3 Tier 4(Manipulation Tasks):	A:NW	1504
1454	single_object_free_obstacle_path_planning (FOP):	Q:Step 1 executed. Continue.	1505
1455	This task is a simplified single-agent grid-navigation benchmark. On obstacle-free discrete grids of four sizes— 3×3 , 5×5 , 7×7 , and 9×9 —the participant must, through multi-turn interaction, sequentially output one of the eight compass directions, guiding the lone object from its given start cell to the target cell. Evaluation focuses on (1) whether the produced path coincides with the shortest path generated by algorithms such as A* or Dijkstra and (2) the model’s decision efficiency and coherence during the interaction. The task’s theoretical foundation traces back to the A* algorithm proposed by Hart, Nilsson, and Raphael in 1968, which first systematized the use of heuristic search for shortest-path planning on regular grids and established the methodological framework for subsequent grid-navigation tasks.	1507
1456		Q:Step n executed. Continue.	1508
1457		A:NONE.Action sequence: NW, NW, NW, NW, NW	1509
1458			1510
1459		obstacle_path_planning_multiturn:	1511
1460		This task evaluates a model’s ability to perform static-obstacle avoidance and shortest-path reasoning in a regular grid environment. It is one of the most classic spatial-reasoning benchmarks and appears widely in robot navigation, reinforcement learning, and, more recently, in planning tests for large language models (Huang et al., 2022). In our setting, the participant must strictly follow the sequence observe \rightarrow orient \rightarrow decide \rightarrow act on maps of four sizes— 3×3 , 5×5 , 7×7 , and 9×9 —step-by-step navigating the object to its destination and, finally, outputting the entire path sequence.	1512
1461			1513
1462			1514
1463			1515
1464			1516
1465			1517
1466			1518
1467			1519
1468			1520
1469			1521
1470			1522
1471			1523
1472			1524
1473			1525
1474	Conversation Examples:		1526
1475	free_obstacle_path_planning_3_multiturn:	Conversation Examples:	1527
1476	Q:Task: 3×3 grid, move from (1, 2) to (0, 0). Output step by step.	single_obstacle_path_planning_3_multiturn:	1528
1477	A:NW	Q:Task: 3×3 grid, move from (1, 1) to (2, 0). Obstacles: $[(0, 1), (0, 2)]$. Output step by step.	1529
1478	Q:Step 1 executed. Continue.	A:SW	1530
1479	Q:Step 1 executed. Continue.	1531
1480	Q:Step n executed. Continue.	A:NONE.Action sequence: SW	1532
1481	A:NONE.Action sequence: NW, W.		1533
1482			1534
1483		obstacle_path_planning_5_multiturn:	1535
1484	free_obstacle_path_planning_5_multiturn:	Q:Task: 5×5 grid, move from (0, 2) to (0, 3). Obstacles: $[(1, 0), (1, 3), (2, 0), (2, 2), (2, 3), (3, 0), (3, 1), (3, 3), (4, 3), (4, 4)]$. Output step by step.	1536
1485	Q:Task: 5×5 grid, move from (4, 2) to (3, 0). Output step by step.	A:E.	1537
1486	A:NW	Q:Step 1 executed. Continue.	1538
1487	Q:Step 1 executed. Continue.	A:NONE.Action sequence: E	1539
1488		1540
1489	Q:Step n executed. Continue.		1541
1490	A:NONE.Action sequence: NW, W.		1542
1491		obstacle_path_planning_7_multiturn:	1543
1492	free_obstacle_path_planning_7_multiturn:	Q:Task: 7×7 grid, move from (3, 6) to (4, 5). Obstacles: $[(0, 1), (0, 2), (0, 5), (0, 6), (1, 1), (1, 2), (1, 6), (2, 0), (2, 1), (2, 2), (2, 4), (2, 5), (3, 3), (4,$	1544
1493	Q:Task: 7×7 grid, move from (5, 5) to (2, 3).		1545
1494			1546

1547	0), (4, 3), (4, 4), (5, 0), (5, 3), (5, 4), (5, 5), (5, 6),	step-by-step.	1599
1548	(6, 3)]. Output step by step.	A:1:SE 2:N 3:SW 4:SE 5:N.	1600
1549	A:SW.	Q:Step 1 executed. Continue.	1601
1550	Q:Step 1 executed. Continue.	1602
1551	A:NONE.Action sequence: SW	Q:Step n executed. Continue.	1603
1552		A:NONE.Total steps: n	1604
1553	obstacle_path_planning_9_multiturn:		1605
1554	Q:Task: 9×9 grid, move from (1, 0) to (1, 1).	Multi-object_control_path_planning_7_multiturn:	1606
1555	Obstacles: [(0, 3), (0, 4), (0, 5), (0, 7), (1, 2), (1,	Q:Task: Synchronously control 7 objects.\nStart	1607
1556	4), (1, 5), (1, 8), (2, 2), (2, 4), (2, 5), (2, 6), (2, 7),	and end points:\n1 (6,4)→(3,3)\n2 (5,5)→(4,3)\n3	1608
1557	(3, 1), (3, 2), (3, 8), (4, 1), (4, 2), (4, 4), (4, 5), (4,	(4,5)→(1,2)\n4 (5,0)→(3,0)\n5 (1,3)→(0,2)\n6	1609
1558	6), (4, 7), (5, 0), (5, 1), (5, 2), (5, 3), (5, 6), (5, 7),	(3,6)→(0,1)\n7 (5,1)→(4,6)\nObstacles: []. Please	1610
1559	(5, 8), (6, 0), (6, 1), (6, 4), (6, 8), (7, 0), (7, 3),	proceed step by step.	1611
1560	(7, 4), (7, 5), (8, 1), (8, 3), (8, 5), (8, 6)]. Output	A:1:N 2:W 3:NW 4:N 5:NW 6:SW 7:NE.	1612
1561	step-by-step.	Q:Step 1 executed. Continue.	1613
1562	A:E.	1614
1563	Q:Step 1 executed. Continue.	Q:Step n executed. Continue.	1615
1564	A:NONE.Action sequence: E	A:NONE.Total steps: n	1616
1565			1617
1566	Multi-object_control_path_planning_multiturn	Multi-object_control_path_planning_9_multiturn:	1618
1567	(obstacle-free version):	Q:Task: Synchronously control 9 objects.\nStart	1619
1568	This task is a “synchronous multi-goal path-	and end points:\n1 (5, 2)→(6, 5)\n2 (1, 1)→(4,	1620
1569	planning task.” On four obstacle-free grid maps—3	3)\n3 (6, 1)→(4, 5)\n4 (1, 8)→(6, 3)\n5 (3, 0)→(2,	1621
1570	× 3, 5 × 5, 7 × 7, and 9 × 9—nine objects (Agents	0)\n6 (2, 2)→(5, 4)\n7 (5, 3)→(3, 3)\n8 (3, 5)→(1,	1622
1571	1–9) must move in lock-step discrete time from	7)\n9 (1, 5)→(4, 7)\nObstacles: []. Proceed step	1623
1572	their individual start cells to their designated goal	by step.	1624
1573	cells while continuously avoiding inter-agent	A:1:NE 2:SE 3:NE 4:SW 5:N 6:SE 7:N 8:NE	1625
1574	collisions. By eliminating static obstacles, the task	9:SE.	1626
1575	isolates the challenges of multi-agent coordination	Q:Step 1 executed. Continue.	1627
1576	and conflict resolution, serving as a direct counter-	1628
1577	part to the obstacle-inclusive version. It therefore	Q:Step n executed. Continue.	1629
1578	enables a systematic assessment of large language	A:NONE.Total steps: n	1630
1579	models’ generalization and reasoning abilities		1631
1580	under different spatial-constraint conditions.	Multi-object_control_obstacle_path_planning	1632
1581		multiturn:	1633
1582	Conversation Examples:	This task requires the participant (or model)	1634
1583	Multi-object_control_path_planning_3_multiturn:	to control multiple objects simultaneously in a	1635
1584	Q:Task: Synchronously control 3 ob-	discrete grid world of five sizes—3 × 3, 5 × 5,	1636
1585	jects.\nStart/End points:\n1 (0, 2)→(0, 1)\n2	7 × 7, 8 × 8, and 9 × 9. All objects must start	1637
1586	(2, 1)→(2, 0)\n3 (1, 2)→(1, 1)\nObstacles: [].	synchronously from their assigned origins, detour	1638
1587	Please proceed step-by-step.	around static obstacles, and eventually reach	1639
1588	A:1:W 2:W 3:W	their respective goals while avoiding inter-object	1640
1589	Q:Step 1 executed. Continue.	collisions throughout the entire process. The task	1641
1590	design follows the well-studied Multi-Agent Path	1642
1591	Q:Step n executed. Continue.	Finding (MAPF) problem in robotics (Standley,	1643
1592	A:NONE.Total steps: n	2010; Stern et al., 2019). By means of this	1644
1593		benchmark, we can systematically evaluate	1645
1594	Multi-object_control_path_planning_5_multiturn:	large language models’ abilities in multi-agent	1646
1595	Q:Task: Synchronously control 5 ob-	coordination, concurrent action generation, and	1647
1596	jects.\nStart/End points:\n1 (2, 1)→(4, 2)\n2	planning reasoning based on structured spatial	1648
1597	(2, 0)→(0, 1)\n3 (1, 4)→(2, 2)\n4 (2, 3)→(4, 4)\n5	representations within a controlled spatial setting.	1649
1598	(3, 2)→(1, 3)\nObstacles: []. Please proceed		1650

weaknesses in how standard LLMs handle complex spatial control. The models' mistakes generally fall into two clear categories: a poor awareness of the board state and a failure to correctly apply game rules. First, the models struggled to maintain an accurate mental map of where the pieces were on the board. This led to "hallucinated" moves based on an incorrect board state. For example, a model might correctly move its knight from g1 to f3 on its first turn. However, several turns later, it might try to move the same knight from g1 again, as if it had completely forgotten the piece had moved. Another common perception error was attempting to move a piece to a square already occupied by one of its own pieces, resulting in an invalid action. Second, the models frequently failed to apply the basic movement rules of chess. They would often generate plans that were physically impossible for a given piece. For instance, a model might try to move a bishop horizontally across the board (e.g., from f1 to c1), a move that is only legal for a rook. They also struggled with more nuanced rules. A frequent error involved pawn movement, where a model would attempt to capture an opponent's piece by moving one square directly forward, instead of capturing diagonally.

C.0.2 Task Setup

To evaluate the model's generalization ability in a complex, multi-step spatial control task, we designed a chess combat test. In this setup, the model plays against Stockfish, a powerful, open-source chess engine widely regarded as a benchmark for chess-playing strength. The experiment is designed not to test grandmaster-level strategy, but rather the model's ability to maintain an accurate internal representation of the board state and consistently adhere to the game's complex rules over a multi-turn interaction.

The game proceeds in turns. For each of its turns, the LLM receives the current board state and is prompted to generate a move. The model is instructed to output its move into the Universal Chess Interface (UCI) protocol, which Stockfish uses for communication. The chess notation used by the Stockfish engine is a coordinate notation based on the Universal Chess Interface (UCI) protocol, known as Long Algebraic Notation (LAN). A game is considered successful if it proceeds until a standard conclusion (e.g., checkmate or stalemate) without the model committing any rule violations. A game is terminated and recorded as a

failure if the model generates an illegal move, such as attempting to move a piece from an incorrect square or violating a piece's movement rules, as detailed in Section C.0.2. Here is one example of Chess_Combat_with_Stockfish:

```
position startpos moves e2e4 e7e5 g1f3 b8c6
f1b5 a7a6 b5a4 g8f6 e1g1 f8e7 f1e1 a6b5 a4b3
d7d6 c2c3 e8g8 h2h3 c6a5 b3c2 c7c5 d2d4 d8c7
b1d2 c5d4 c3d4 c8d7 a2a4 b5a4 a4a5 d7d7 b2b4
a5c6 e5e9
```

In this practical example, the UCI engine will reject or ignore an illegal move like e5e9(11m), so the program needs to detect it and declare the game ended due to an LLM violation. It does not count as the LLM having completed the game.

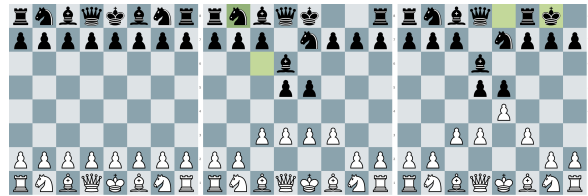


Figure 6: The Chess Combat evaluation setup visualization. The LLM (white) processes the board state to generate a move in standard notation, which is then played against the Stockfish engine (black).

D Detail of Robot Control

D.0.1 Task Setup

The experimental environment consisted of a 6-DoF robotic arm operating over grid-based mazes of varying sizes (3x3, 5x5, 7x7, and 9x9) and a local server equipped with two NVIDIA RTX 4090 GPUs. The maze contained a single target object, one or more static obstacles, and a designated target location. The task required the robotic arm to pick up a target object and transport it to a designated location, navigating around static obstacles while adhering to a strict set of movement rules.

D.0.2 Control Flow

We designed a text-only control system that operates as an iterative, closed-loop process. The workflow for each decision cycle is as follows:

- State and Rule Encoding:** At the beginning of each decision cycle, the system receives the current world state including object, target, and obstacles location. This world state information is then encoded into a structured textual format. This state description is combined with a set of predefined rules and con-

Trial ID	Obstacles	Model	Result	Path Length	Avg. Step Latency (s)
1	2	Qwen-4B	Failure (Collision)	-	7.1
2	2	SODA-4B	Success	6	8.8
3	3	Qwen-4B	Success	8	7.5
4	3	SODA-4B	Success	7	9.0
5	4	Qwen-4B	Failure (Collision)	-	7.4
6	4	SODA-4B	Success	7	9.3
7	5	Qwen-4B	Failure (Invalid Move)	-	7.6
8	5	SODA-4B	Success	8	9.5

Table 7: Parts of Detailed Trial Log for 5x5 Robotic Arm Task

Model	Success Rate (%)	Avg. Path Length (steps)	Avg. Step Latency (s)
Qwen-4B	35	6.4	7.5
SODA-4B	90	7.6	9.1

Table 8: Aggregated Performance on the 5x5 Robotic Arm Task

1823 straints to form a comprehensive prompt for
1824 the LLM. For example:

1825 State: Arm at (pointA). Object at (pointB).
1826 Obstacle at (pointC). Target at (pointD). Task:
1827 Move object to target, avoid obstacle. Rule:
1828 There are three operations to choose: Move,
1829 Pickup and drop. Move only one grid horizon-
1830 tally or vertically each step.

- 1831 2. **LLM-based Planning:** The LLM processes
1832 this prompt to determine and generate the single
1833 most appropriate action for the current
1834 step. The model’s output is a discrete, low-
1835 level command consisting of an action type
1836 and its corresponding coordinates. For exam-
1837 ple:

1838 Plan: 1. move(point1) 2. pick(point2) 3.
1839 move(point3) 4. drop(point4)

1840 rated command is parsed and translated into
1841 motor commands for the robotic arm. After
1842 the action is physically executed, the entire cy-
1843 cle repeats from the first step: the system gets
1844 the new world state, generates a new prompt,
1845 and queries the LLM for the next action. This
1846 iterative process continues until the model is-
1847 sues a final command that completes the task.

1848 D.0.3 Error of Robot Control

1849 The llm-based robotic arm task revealed a signif-
1850 icant gap between the baseline model’s abstract
1851 reasoning and the requirements of physical embod-
1852 iment. The failures of the untrained model were not
1853 random but systematic, highlighting fundamental
1854 deficits in its ability to ground symbolic plans in a

1855 constrained physical environment. The errors ob-
1856 served fall into three categories: firstly, The model
1857 frequently generated plans that resulted in direct
1858 collisions. For instance, given an obstacle at [3,3],
1859 the model would still output move [3,3] as part of
1860 a path. This indicates a critical breakdown in the
1861 Orient phase, where the model failed to incorpo-
1862 rate the explicit obstacle locations from the prompt
1863 into its internal world model, treating the task as an
1864 unconstrained pathfinding problem. Secondly, The
1865 model struggled to adhere to the kinematic rules
1866 defined in the prompt. Despite being explicitly
1867 forbidden, it often generated kinematically invalid
1868 actions, such as diagonal moves (e.g., move [1,1]
1869 from [0,0]) or multi-cell jumps (e.g., move [0,2]
1870 from [0,0]). This suggests its internal action gen-
1871 eration mechanism defaults to generalized notions
1872 of movement rather than the specific, constrained
1873 action space of the task. Thirdly, The model ex-
1874 hibited a poor ability to track its own state within
1875 the task sequence. This often led to a collapse of
1876 the planning process, where the model would get
1877 "stuck" in a repetitive loop (e.g., repeatedly out-
1878 putting move [1,2] followed by move [1,3]). This
1879 behavior demonstrates a failure to form a coherent,
1880 long-term plan and an inability to recognize that
1881 its current strategy was making no progress toward
1882 the final goal.

1883 D.0.4 Experimental Results

1884 To quantify the advantages of the SODA framework
1885 in a physical embodiment task, we conducted a se-
1886 ries of simulated experiments on the 6-DoF robotic
1887 arm. The experimental environment consisted of a

1888 UR5e robotic arm operating over grid-based mazes
1889 of varying sizes (5x5) and a local server equipped
1890 with an NVIDIA RTX 5090 GPU (32GB VRAM).
1891 The maze contained a single target object, one or
1892 more static obstacles, and a designated target lo-
1893 cation. The task required the robotic arm to pick
1894 up a target object and transport it to a designated
1895 location, navigating around static obstacles while
1896 adhering to a strict set of movement rules.

1897 We compared our SODA-4B model against the
1898 baseline Qwen-4B model across 50 trials of varying
1899 complexity. Detailed records for a subset of these
1900 trials are shown in Table 7, and the aggregated
1901 results are presented in Table 8.

1902 The results demonstrate a substantial perfor-
1903 mance improvement in the SODA-4B model. With
1904 a 90% success rate, SODA-4B significantly outper-
1905 formed the baseline Qwen-4B (35%). The base-
1906 line model’s failures were consistent with the error
1907 types previously described: collisions with obsta-
1908 cles, generation of kinematically invalid moves,
1909 and getting trapped in repetitive action loops. The
1910 high success rate of SODA-4B indicates that its en-
1911 hanced spatial reasoning, derived from the OODA
1912 framework, effectively mitigates these issues in a
1913 constrained physical environment.

1914 Furthermore, SODA-4B demonstrated greater
1915 planning efficiency. In successful trials, it com-
1916 pleted the task with an average path length of 7.8
1917 steps, compared to the baseline’s 6.4 steps. This
1918 suggests that SODA prefer to succeed since 8 steps
1919 means final goal-arriving in grid(5x5).

1920 Interestingly, the enhanced reliability and effi-
1921 ciency of SODA-4B came with a slight increase
1922 in decision latency, averaging 9.1 seconds per step
1923 versus Qwen-4B’s 7.5 seconds. This modest trade-
1924 off is attributable to the model’s more deliberate
1925 OODA-based reasoning process, which involves
1926 deeper analysis during the Observe and Orient
1927 phases before acting. The significant increase in
1928 task success and planning efficiency justifies this
1929 marginal increase in processing time.

1930 In a nutshell, these results validate that the
1931 SODA framework successfully bridges the gap
1932 between abstract reasoning and embodied intelli-
1933 gence, enabling the model to generate robust, effi-
1934 cient, and physically-grounded plans for complex
1935 robotic control tasks.